MRC/ABQ-R-1450
Copy 1

Mission Research Corporation

COMPACT-BEAM STABLE-UNSTABLE RESONATOR FOR FREE-ELECTRON LASER (PHASE II FINAL REPORT)

A.H. Paxton
C.J. White
T.L. Boyd
M.J. Schmitt
C.H. Aldrich

October 1991

Prepared for: Los Alamos National Laboratory
P.O. Box 990
Los Alamos, NM 87545

Work sponsored by: Strategic Defense Initiative Organization

Prepared by: MISSION RESEARCH CORPORATION
1720 Randolph Road, S.E.
Albuquerque, NM 87106-4245

COMPACT-BEAM STABLE-UNSTABLE RESONATOR FOR FREE-ELECTRON LASER (PHASE II FINAL REPORT)

A.H. Paxton
C.J. White
T.L. Boyd
M.J. Schmitt
C.H. Aldrich

October 1991

Prepared for: Los Alamos National Laboratory
P.O. Box 990
Los Alamos, NM 87545

Work sponsored by: Strategic Defense Initiative
Organization

Prepared by: MISSION RESEARCH CORPORATION
1720 Randolph Road, S.E.
Albuquerque, NM 87106-4245

CONTENTS

DISCLAIMER

1.0 INTRODUCTION

In addition to this report, two publications discuss work performed under this contract. Reprints are included in Appendix A. The work documented in them is not included in the main body of this report. We wish to thank Bernadette Lerma for her expertise in typesetting this report.

A significant problem in the design of high-energy free-electron lasers (FELs) centers on the technique for outcoupling the output beam. FELs with currently achieveable output power usually include a conventional stable resonator with output through a partially transmitting mirror. This outcoupling method will not work for arbitrarily high average power, so an alternate scheme must be found for high-energy FELs. A high-efficiency grating outcoupler is an attractive possibility because it can be included as an element of a grating rhomb to suppress the sideband radiation[1], but it is difficult to manufacture, particularly because it must withstand high average optical flux without suffering severe thermal distortion nor damage. Other suggestions include unstable resonators with an intracavity focus[2-5] and unstable resonators with an intracavity focus and beam rotation.[6] The intensity distribution at the intracavity focus of a negative-branch unstable resonator has side-lobes that would be scraped off by the faces of the wiggler magnets or by the beam tube through the wiggler, because the space between the faces of the wiggler magnets is too small to pass the side lobes and still allow the main lobe to have the optimum size for interaction with the electron beam.[5] The resulting power loss would be significant. Therefore, it is desirable to develop another type of resonator for use with FELs.

The resonator that we have developed under this project is the compact-beam stable-unstable ring resonator (CBSUR). It is a stable resonator in one transverse dimension and an unstable resonator with an intracavity focus in the orthogonal transverse dimension. A scraper mirror outcouples the output beam from one side of the mode only. The resonator can be configured so that it has a small beam waist at the center of the wiggler in the stable direction and has an intracavity focus in the unstable direction. The half-width of the central lobe of the focus is approximately the size of the

stable beam waist. In the stable direction, the Gaussian amplitude distribution results in a small loss on the wiggler magnets, or on a beam tube that will fit within the wiggler, if one is used. The beam tube can have an elliptical shape to permit the passage of several side lobes in the unstable dimension. We have published the results of the numerical calculation of modes of the CBSUR[7]. A reprint is included in Appendix A.

The integral equation is separable in cartesian coordinates for the bare-cavity modes of an orthogonal[8] resonator if the dominant apertures are rectangular. Therefore, a mode of the CBSUR is a product of the mode of a strip stable resonator with a strip compact-beam negative-branch unstable resonator, and the properties of these two resonators also apply to the CBSUR.

The negative-branch unstable resonator is not an off-axis resonator in the usual sense that is applied to positive branch resonators. The output beam is scraped off only one side of the intracavity beam, but the optic axis is well within the geometric beam, and diffraction losses are not significant at the side of the beam opposite the scraper mirror. This is because the light rays cross to the opposite side of the resonator each round-trip pass, so the scraper mirror limits the beam on both sides of the mode even though only one side is clipped. This is in contrast to the positive-branch off-axis unstable resonator that has been studied previously.[9,10] The use of a negative-branch strip resonator with a single-sided scrape was independently suggested by Jones, Cason, and Perkins for use in one or both transverse dimensions of an FEL[11], subsequent to the submission of our proposal for this project in Feb. 1987. It was also independently proposed by A.E. Siegman.[12] This resonator has been shown in our previous work to have the same modes as the unstable resonator with 90° beam rotation, and its properties were discussed and modes were calculated for application to that geometry.[13,14]

The geometry of the stable dimension is constrained by the requirement that the beam width at the mirrors must be much larger than at a beam waist. The stable dimension is an almost confocal stable ring resonator. This resonator was shown to be much less sensitive to mirror tilt than its standing-wave counterpart, the almost concentric stable resonator.[15]

Geometric Properties of Experimental CBSUR

We tested a CBSUR, but with the laser gain provided by a flashlamp-pumped dye cell rather than an electron beam. We wanted to determine whether the resonator would operate with nearly diffraction limited beam quality and to determine the sensitivity to mirror tilt for comparison with values from simple ray-optical equations and from laser simulation codes.

Our initial intent was to perform the experiments using a cylindrical telescope to provide beam expansion in the unstable dimension. We were unable to obtain cylindrical mirrors or lenses with the appropriate focal lengths, so we decided to introduce astigmatism at spherical mirrors to differentiate between the stable and unstable dimensions. A top view of the resonator is shown in Fig. 1. This projection shows the unstable dimension of the resonator. It is convenient to use a separate coordinate system for each segment of the resonator, as is shown in Fig. 1. The z coordinate is always along the direction of propagation of the mode, and y is always vertical. The angle of incidence of the resonator beam was 10° at both of the spherical mirrors. The focal length for tangential rays, which applies to the unstable dimension, is

$$f_t = r\cos(\theta)/2 = 344.68 \tag{1}$$

and the focal length for saggital rays, which applies to the stable dimension, is

$$f_s = r/(2cos(\theta)) = 355.40 \tag{2}$$

The angle was selected to allow stable operation in the y dimension, with a beam size of about $w = 5$ mm in the expanded region, Region 2. The other goal was unstable operation in the x dimension, with resonator magnification around $M = 1.3$ or $M = 1.4$. The condition for stable-unstable operation was, $f_t < L_1/2 < f_s$.

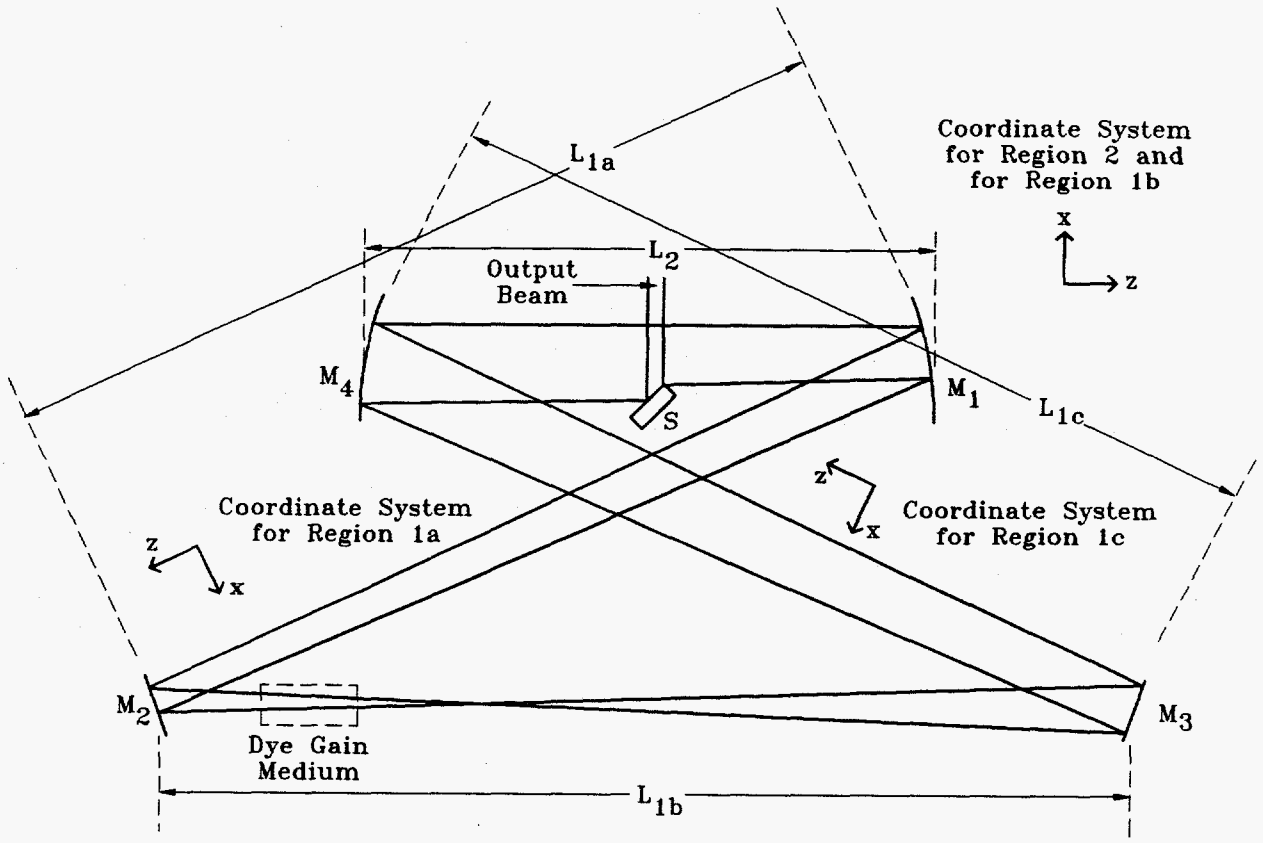

Figure 1. Top view of compact-beam stable-unstable resonator (CBSUR). Light rays at the geometric edges of the beam are shown. It is apparent that the scraper mirror also limits the edge of the beam opposite it because the rays change sides each round trip. The mode reflects from each of the two spherical mirrors, M_1 and M_4, with a 10° angle of incidence. Their focal lengths are both 350.0 cm. The off-axis angle results in an effective focal length of $f_t = 344.7$ cm for rays in the tangential plane (the x, z plane), which are shown in this projection. The dimensions for the initial setup were $L_{1a} = L_{1c} = 220.79$ cm, $L_{1b} = 268.42$ cm, and $L_2 = 146.52$ cm. After setting up the resonator with these dimensions, the desired stable beam width of $w = 0.49$ cm in Region 2 was obtained by moving Mirrors M_1 and M_2 outward by 1.975 cm each giving $L_{1a} = 224.50$ cm, $L_{1b} = 270.4$ cm, $L_{1c} = 220.79$ cm, and $L_2 = 148.50$ cm. This design can be modified to locate the tangential-plane focus at the saggital-plane beam waist by replacing M_3 with a cylindrical mirror; see Fig. 22.

Beam Geometry in Stable Dimension

A y, z projection of the resonator, with the spherical mirrors shown as lenses, is sketched in Fig. 2. This projection shows the stable dimension. The stable-resonator mode is symmetrical about the two planes where the beam waists occur. The equations for the propagation of a Gaussian beam can be used to derive the Gaussian-beam widths in the vertical dimension at various locations in the resonator. A first-order treatment was given in Ref. 15. An exact unobsecured Gaussian-beam treatment results in a significant difference for the geometry of our experiment, so we apply it here. We will now derive the equations for the sizes of the two beam waists. Once these are known, the Gaussian-beam size at any plane in the resonator can be found. Region 1 has a symmetrical mode with beam size w_m at mirrors M_1 and M_4, and Region 2 has a symmetrical mode with beam size w_m at mirrors M_1 and M_4. The radius of curvature C_1 of the wavefronts of the optical beam immediately adjacent to mirror M_1 in Region 1 must be related to the radius of curvature C_2 of the wavefronts immediately adjacent to mirror M_2 in Region 2 by the equation,

$$\frac{1}{C_1} + \frac{1}{C_2} = \frac{1}{f} \tag{3}$$

Applying these conditions, we obtain the g parameters for the equivalent standing-wave resonators,

$$g_1 = \frac{1}{2L_2}\left[L_1 + L_2 - \frac{L_1 L_2}{f} + \frac{L_2^2 - L_1^2}{L_1 + L_2 - \frac{L_1 L_2}{f}}\right] \tag{4}$$

where g_2 is obtained by interchanging L_1 and L_2 in Eq. 4, and the g parameters are defined to be

$$g_i = 1 - L_i/R_i \tag{5}$$

The usual equation for the beam waist in a symmetrical resonator applies,

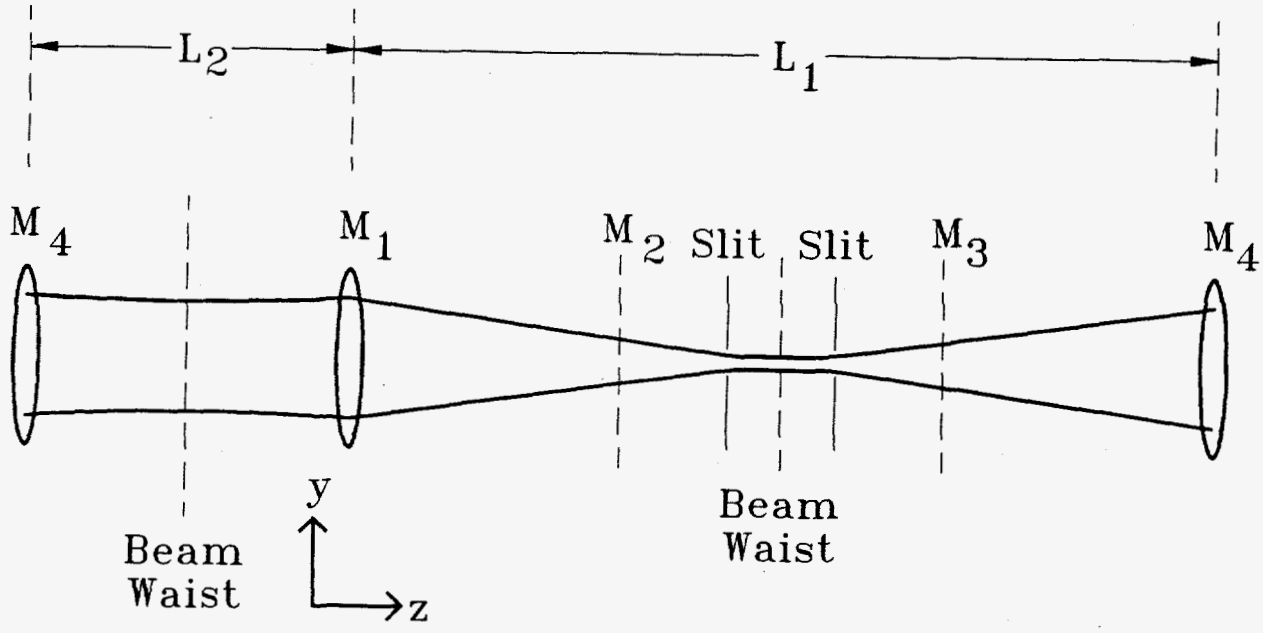

Figure 2. The envelope of the light beam that constitutes the laser mode shown in the saggital planes (the y, z planes). The envelope of the beam at the distance of the Gaussian beam half-width, w, from the central axis is traced by two lines. One period of the periodic lens train equivalent to the resonator is shown. The effective focal length of each of the two concave mirrors for light rays in the saggital planes is 355.4 cm. The unperturbed resonator has a small beam waist at the center of Region 1 and has a large waist at the center of Region 2. The beam is effectively collimated in Region 2 because its Rayleigh range is orders of magnitude larger than L_2.

$$w_{oi}^2 = \frac{L_i \lambda}{\pi} \sqrt{\frac{1+g_i}{1-g_i}} \tag{6}$$

as does the usual equation for the beam size where the end mirrors would be in the equivalent standing-wave resonators, at M_1 and M_4,

$$w_i^2 = \frac{L_i \lambda}{\pi} \sqrt{\frac{1}{1-g_i^2}} \tag{7}$$

Plots of the sizes of the beam waists as a function of the segment lengths, L_1 and L_2, provide an indication of the sensitivity of the mode geometry to variations in these parameters. The beam waist in the shorter segment is always larger. Figure 3 shows the size of the small waist as a function of L_1 for three values of L_2. The middle value of L_2 was the value initially selected for the experiment. The small waist size approaches zero as L_1 approaches $2f_s$, while it is not particularly sensitive to changes in L_2, provided that L_2 is enough smaller than L_1. Curves of the large waist size as a function of L_1 are shown in Fig. 4. The large waist size approaches infinity as L_1 approaches $2f_s$.

Beam Geometry in Unstable Dimension

An $x-z$ projection of the resonator mode is shown in Fig. 5. The unstable mode has an intracavity focus at point c_1, and the center of curvature of the mode in Region 2 is located at c_2. The geometry of the mode is derived from the conditions that the image of c_1 seen in Mirror M_4 is at c_2, and the image of c_2 seen in Mirror M_1 is at c_1. Thus,

$$\frac{1}{d_1} + \frac{1}{d_2} = \frac{1}{f_4} \tag{8}$$

and

$$\frac{1}{L_2 - d_2} + \frac{1}{L_1 - d_1} = \frac{1}{f_1} \tag{9}$$

The solution is

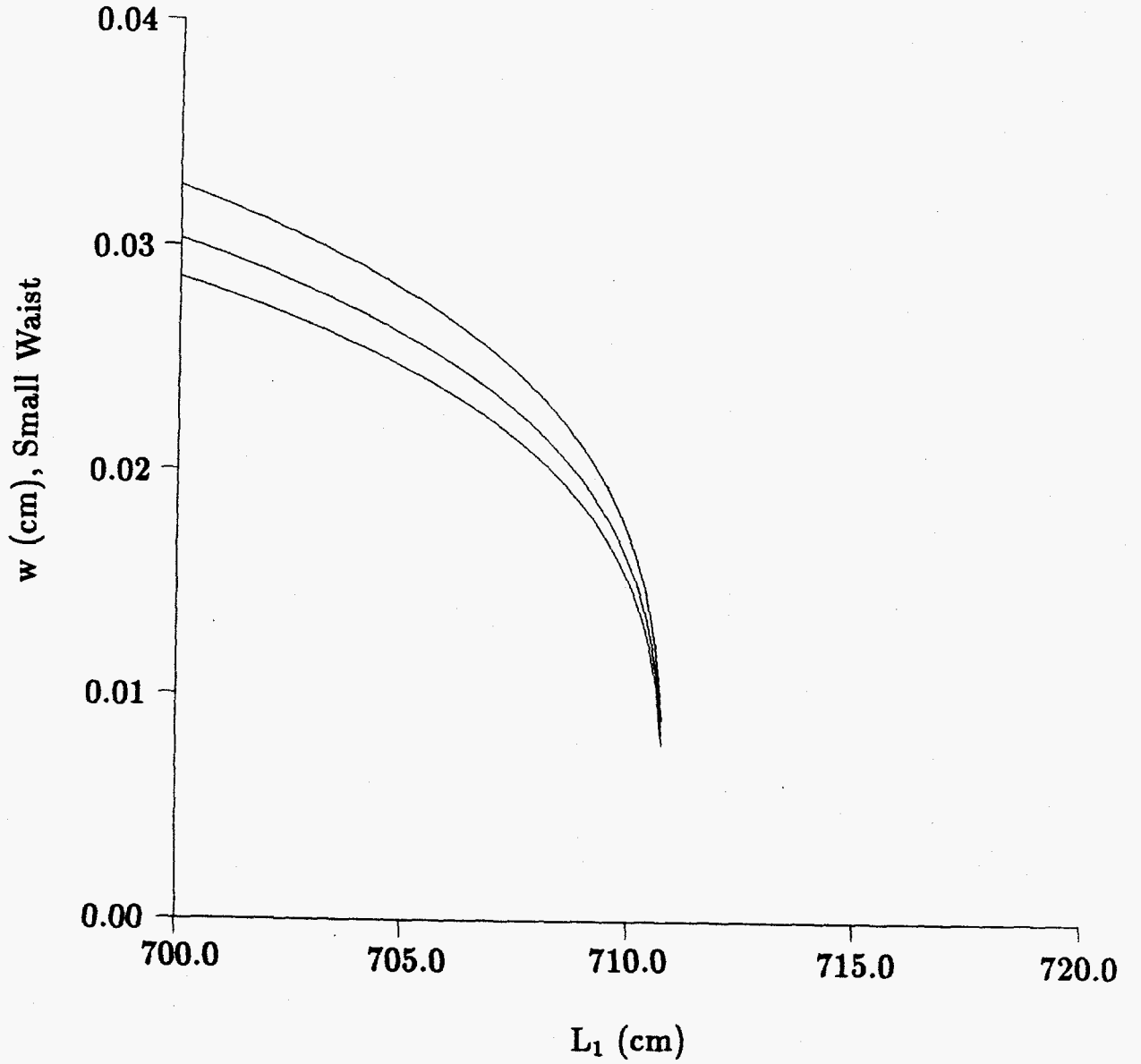

Figure 3. Curves showing the size of the small waist as a function of L_1. The values of L_2 from bottom to top are 2.0 cm, 146.5 cm, and 291.0 cm. The middle curve corresponds to the initial configuration for the resonator. The waist size approaches zero as L_1 approaches twice the effective focal length of the mirrors.

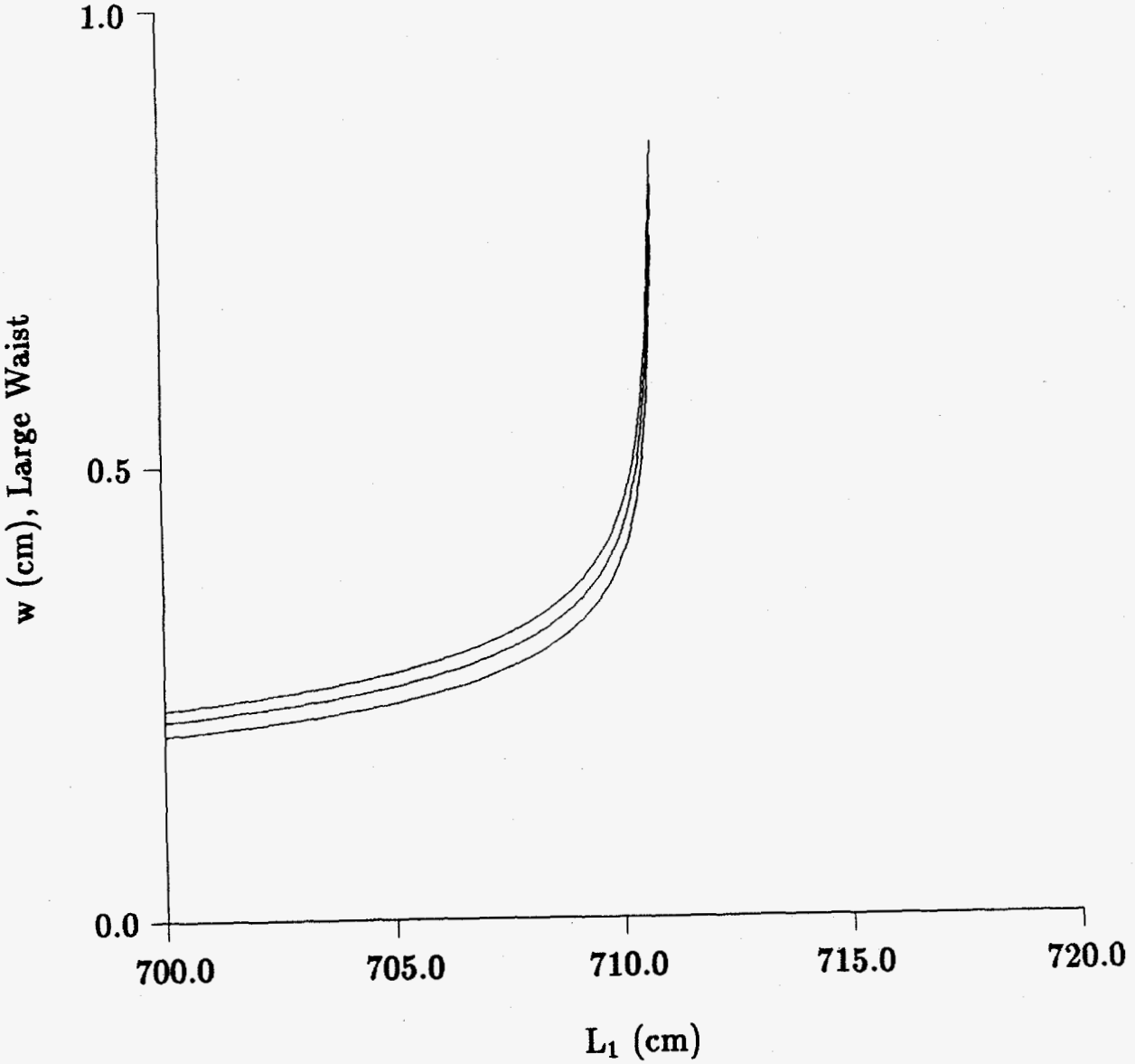

Figure 4. Curves showing the size of the large waist as a function of L_1. The values of L_2, from bottom to top are 291.0 cm, 146.5 cm, and 2.0 cm. The middle curve corresponds to the initial configuration for the resonator.

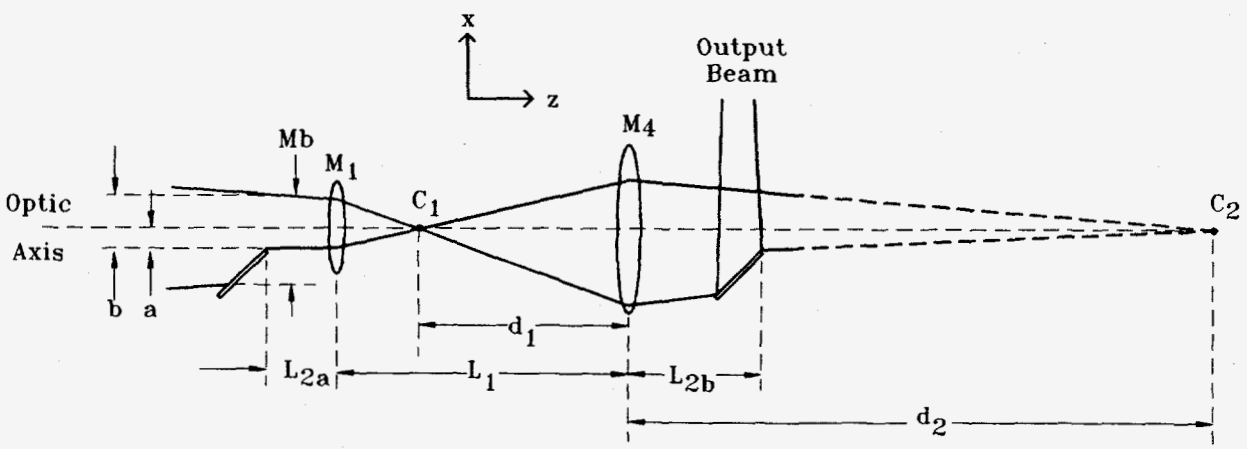

Figure 5. One period of the periodic lens train equivalent to the tangential plane of the resonator. The geometric optical size of the feedback beam is b, and the size of the beam incident on the outcoupling plane is Mb in this dimension. The center of curvature of the light beam in Region 2 is at c_2, and the intracavity focus is at c_1.

$$d_2 = (-B + \sqrt{B^2 - 4AC})/2A \tag{10}$$

where

$$\begin{aligned} A &= f_1 - L_1 + f_4 \\ B &= L_1 f_4 - L_2 f_1 - L_2 f_4 - L_1 f_1 + L_1 L_2 \\ C &= L_2 f_1 - L_1 L_2 + L_1 f_1 \end{aligned} \tag{11}$$

The magnification of the resonator is defined to be the beam width immediately before the scraper mirror divided by the beam width immediately after the scraper mirror, as shown in Fig. 5. It is given by

$$M = \frac{d_1(d_2 - L_2)}{d_2(d_1 - L_1)} \tag{12}$$

Curves of the magnification as a function of L_2 are shown in Fig. 6. The curves correspond to three different values of L_1, and the middle curve corresponds to the initial design for the resonator.

An important geometrical parameter of the unstable resonator mode is the equivalent Fresnel number. The equivalent Fresnel number is indicative of the influence of diffractive effects on the resonator mode. A higher equivalent fresnel number indicates that the intensity of the optical beam falls off more sharply at its geometric edges. The feedback ratio as a function of the equivalent Fresnel number, with the magnification kept constant, is quasiperiodic with local maxima near half-integer values. The difference between the bare-cavity feedback ratios of the lowest loss and second lowest loss modes is also a maximum for values of the equivalent Fresnel number near half-integers.

To illustrate the dimensions that determine the equivalent Fresnel number, Fig. 7 shows the projection of the laser beam on the x, z plane with dimensions labeled that are not

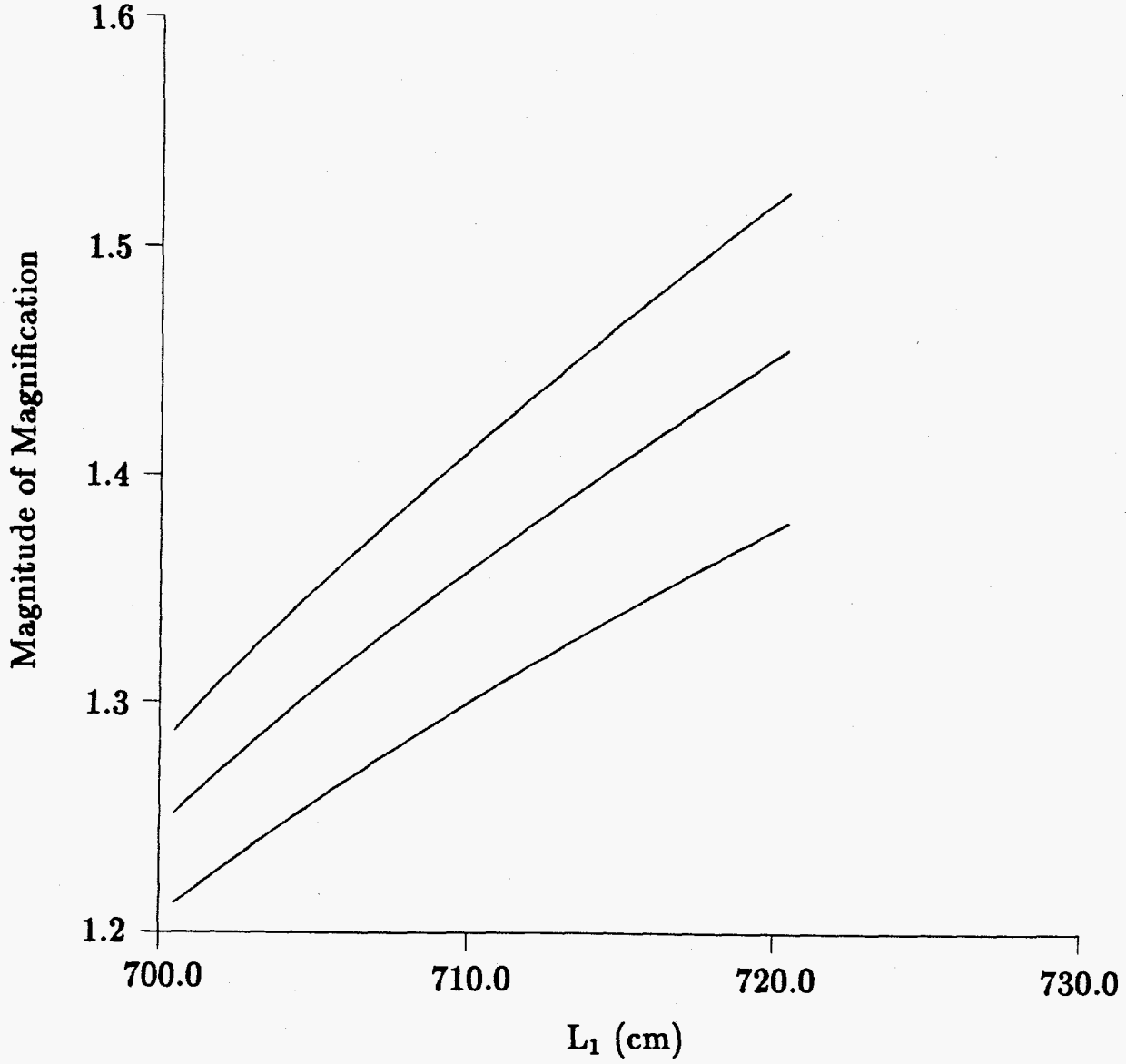

Figure 6. Magnitude of resonator magnification, M, as a function of L_1 for three values of L_2. The values of L_2 from bottom to top are 291.0 cm, 146.5 cm, and 2.0 cm. The magnification is negative.

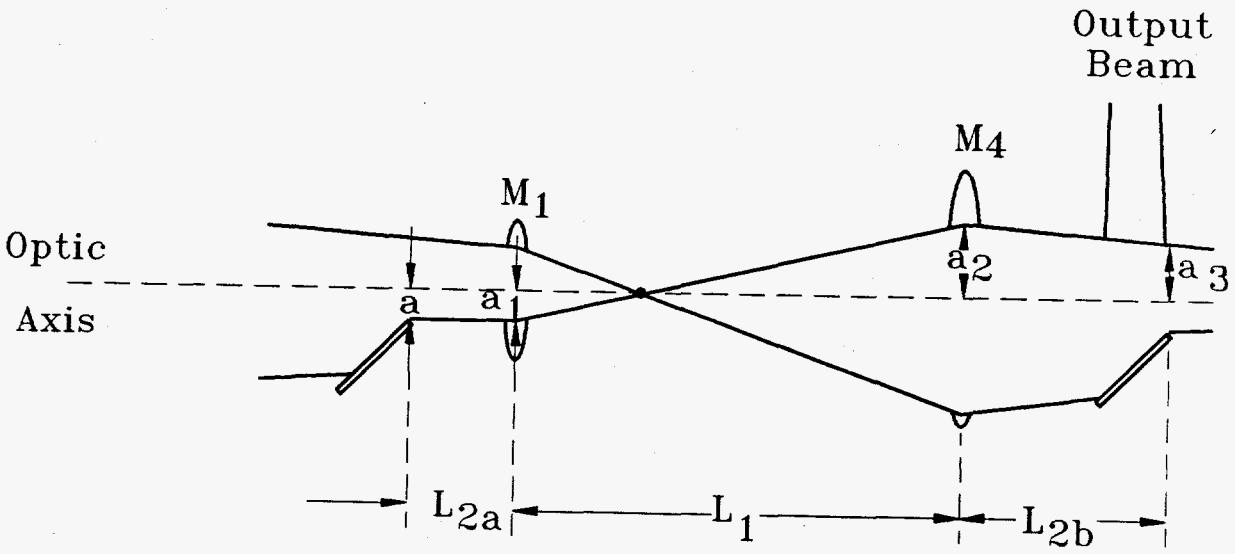

Figure 7. One period of the periodic lens train equivalent to the tangential plane of the resonator. The transverse geometric optical beam sizes at various planes are shown. These are used in calculating the equivalent Fresnel number.

shown on Fig. 5. A Fresnel number can be defined for each beam segment with a constant center of curvature. From left to right starting with the scraper mirror, they are

$$N_1 = \frac{aa_1}{\lambda L_{2a}} \tag{13}$$

$$N_2 = -\frac{a_1 a_2}{\lambda L_1} \tag{14}$$

and

$$N_3 = \frac{a_2 a_3}{\lambda L_{2b}} \tag{15}$$

The overall Fresnel number for the resonator is

$$\frac{1}{N_r} = \frac{1}{N_1} + \frac{1}{N_2} + \frac{1}{N_3} \tag{16}$$

and the equivalent Fresnel number can be defined in terms of the overall Fresnel number

$$N_{eq} = \frac{(M^2 - 1)N_r}{2M^2} \tag{17}$$

Equations 16 and 17 clearly apply to conventional symmetrical resonators.[16] The fundamental derivation of the equivalent Fresnel number for negative-branch resonators with a compact output beam is given in Ref. 14. Equation 17 gives the same result as this derivation. The derivation in Ref. 14 is based on Anane'ev's explanation[17] of the quasi-periodicity of the resonator eigenvalue based on the phase of the ray of the edge wave from the feedback aperture that goes into the converging wave of the resonator. The equivalent Fresnel number of the design for our experimental stable-unstable resonator is $N_{eq} = -1.3$.

A resonator with a negative equivalent Fresnel number has the same intensity distribution and eigenvalue spectrum as a resonator with a positive value with the same magnitude.[3] Curves showing the magnitude of the equivalent Fresnel number as a

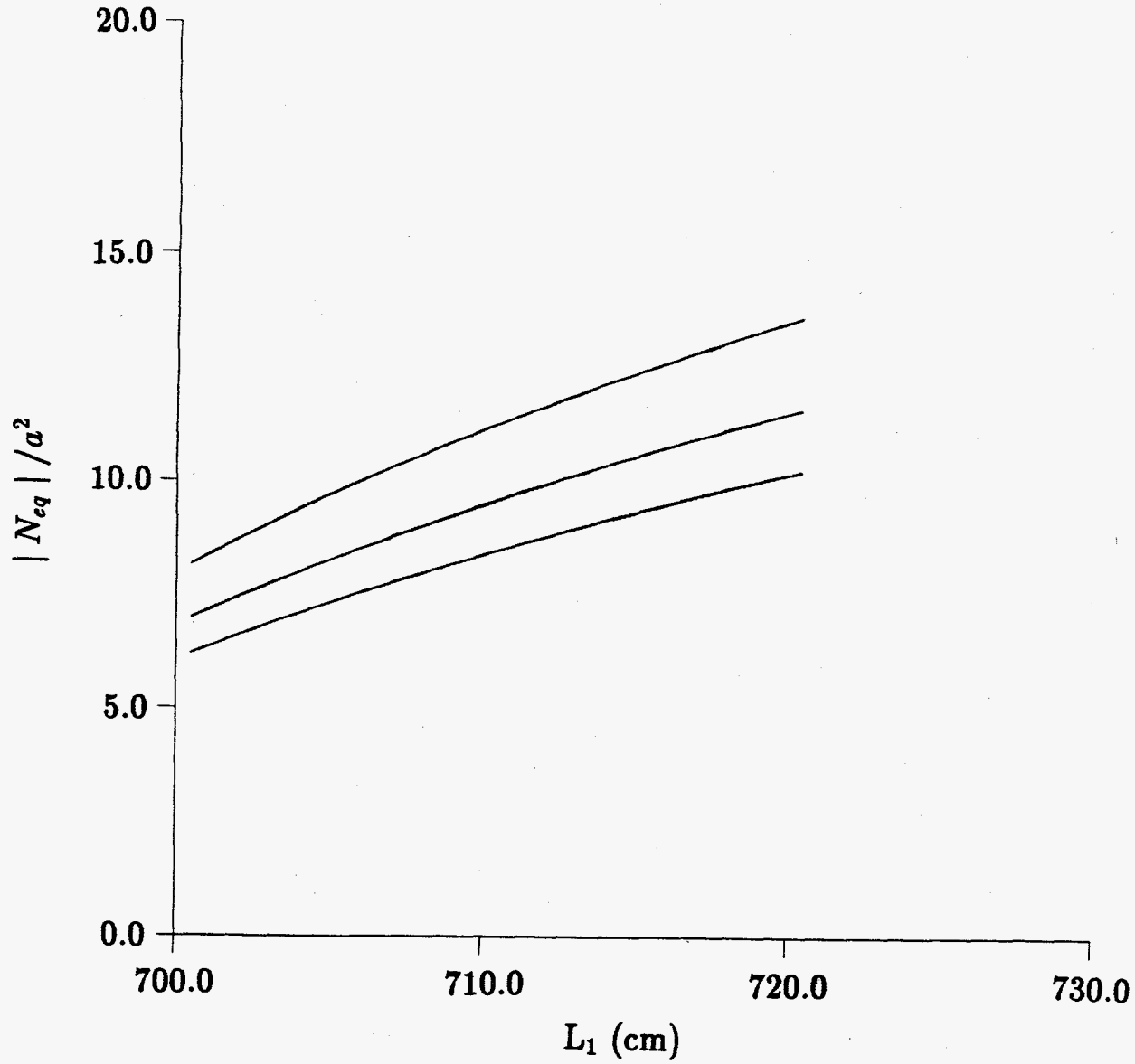

Figure 8. Magnitude of equivalent Fresnel number divided by a^2 as a function of L_1 for three values of L_2. The scraper mirror was assumed to be located 2/3 of the way from Mirror M_4 to Mirror M_1. The precise values of L_{2a} and L_{2b} used in the experiment were not measured. The values of L_2 from bottom to top are 2.0 cm, 146.5 cm, and 291.0 cm. The equivalent Fresnel number is negative.

function of L_2 are given in Fig. 8. The three curves correspond to three values of L_1; the middle curve corresponds to the design value for the resonator.

Experimental Configuration

For misalignment experiments, the apertures at the two ends of the wiggler were simulated by two slits with diameter 0.056 cm placed 14 cm on either side of the small beam waist. The size of the small beam waist for the experimental configuration was $w_0 = 0.0135$ cm, and the beam size at the apertures was $w_a = 0.024$ cm.

The resonator was stable in the vertical dimension and unstable with a magnification of $M = 1.37$ in the horizontal dimension. Figure 1 shows the resonator viewed in the horizontal plane. Figure 2 shows the unfolded resonator viewed in vertical planes that contain the optic axis.

The output beam was taken from one side of the beam only by an output scraper mirror. To minimize the effect of the scraper edge on the beam quality, a mirror segment fabricated for use in a segmented adaptive mirror was used. The segment was a 1.65 cm square dielectric coated flat with better than $\lambda/40$ rms surface figure, averaged over the entire aperture (as opposed to the usual specification over the central 80% of the clear aperture). The substrate blank was machined to $\pm$ 0.0005", with no bevel, chip, or edge irregularities of more than 0.001". The outcoupled beam was rectangular, measuring approximately 1.0 cm in the vertical and 0.2 cm in the horizontal. These dimensions are determined by the size of the stable mode at the scraper and by the unstable-resonator magnification and the distance from the optic axis to the edge of the scraper mirror, respectively. The beam is nearly collimated in the region between M_1 and M_4, in which the scraper is positioned.

The gain medium was a coaxial flashlamp-pumped Candela SLL-500 pulsed dye laser, operating on a 2.0×10^{-5} molar concentration of R-590 perchlorate in a 50/50 mix of reagent grade methanol and water. The SLL-500 comes with a standard Fabry-Perot resonator consisting of two flat mirrors, one of them with 20% reflectivity. In this standard configuration, the laser characteristics are listed in Table 1.

TABLE 1	
Wavelength	590 nm
Output energy*	1.25 J/pulse
Maximum repitition rate	0.5 Hz
Pulse duration	500 ns
Divergence	2.5 mr
Length of gain region	43.2 cm

* Operation at derated flashlamp input for increased lamp life.

The standard flat-flat resonator was removed and the CBSUR was constructed with $\lambda/20$ flats and $\lambda/10$ concave mirrors, dielectrically coated for a center wavelength of 590 nm. M_2 and M_3 were 2" flats. M_1 and M_4 were concave mirrors that were 2" in diameter with the same focal length of 350.0 $\pm$ 0.5 cm. A Foucault knife-edge measurement was made to verify the focal lengths and surface figures of the spherical mirrors.

The small Gaussian-beam waist in the stable dimension occurred approximately halfway between M_2 and M_3 and was predicted to be $w_0 = 0.0158$ cm for the initial resonator. The final resonator dimensions were dictated by physical constraints imposed by the table area, available optics, and the need to keep the beam waist out of the dye cell. Due to the pumping distribution of the flowing dye, some lensing occurred in the gain medium, with the effective focal length changing during the pulse. Care was taken to prevent damage to the laser head due to this effect.

To compensate for the effect of the index of refraction of the dye and the lensing effect, the length of the resonator was expanded by translating mirrors M_1 and M_2 parallel to the axis between M_2 and M_3. The resonator was expanded along this axis until the stable-unstable condition was observed. The beam diameter expanded dramatically in the region between M_1 and M_4 when the stable-unstable condition obtained. Near the stable-unstable condition, adjustment of the mirrors by just a few mm made a large

difference in the beam width in this region. When the resonator was running stable-stable, prior to adjustment of the ring perimeter, the beam half-width in at mirror M_1 in the stable dimension was $w = 0.1$ cm. Upon achieving the proper compensation for the refractive index in the circulating dye, a half-width of $w = 0.49$ cm was obtained. A value close to $w = 0.5$ cm was desired. It was demonstrated that, despite the extreme sensitivity of the resonator to the length between the concave mirrors of the region with the small beam waist, the resonator could be adjusted to compensate for perturbations with magnitudes that were not precisely known.

Rough alignment was achieved by passing the output from a 1.5 mW Lansing HeNe alignment laser through the back of M_4 at the location desired for the optic axis. The mirrors were adjusted until the HeNe beam was centered on the mirror surfaces and through the gain tube. Then a final adjustment was made to cause the beam to reproduce its path after a round trip in the resonator. The optic axis was kept planar to within a tolerance of 0.5 mm.

The lowest flashlamplamp voltage for which lasing occurred reliably was 17 kV. The experiments were done at a slightly higher voltage to preserve the low-power dielectrec coatings on some of the mirrors.

Output Energy and Near-Field Intensity Distribution

A slit was placed at the small beam waist of the resonator. It was oriented horizontally to reject nonzero order modes in the stable dimension. The position and size of the slit were adjusted to maximize the output energy while obtaining an intensity distribution at M_1 corresponding to a Gaussian beam. It was found that a slit width of 0.4 mm worked well. We measured the pulse energy and spatial distribution of the laser output, and the spatial and temporal distribution of the field at M_1.

We studied the temporal behavior of the resonator using EG&G FND-100Q photodiodes on fast 50 Ω microstriplines and an internally triggered Tektronix 7844 dual-beam storage scope. With the microstripline configuration, the FND-100Q has a rise time of < 1 ns and a response of 0.4 A/W at 590 nm with a 70 V bias. With a 50 Ω load, its

response is 0.02 V per 1 mW of incident laser light. The temporal developement of sidelight fluorescence from the dye head is shown in Fig. 9. The power near M_1 is shown in Fig. 10.

The output pulse energy was measured with a Gentech E200 energy detector and a PRJ-A monitor. Lasing occurred in both directions around the ring. Output properties were obtained for both directions by changing the position and orientation of the scraper mirror. Beam profiles were essentially the same, but the output energy measured in the direction indicated in Fig. 1 was approximately 1.5 mJ per pulse higher. All measurements were made using this scraper position unless otherwise noted. The pulse energy with the scraper in this position was 8.30 mJ $\pm$ 0.05 mJ, corresponding to approximately 16.6 kW power averaged over the pulse length. Measurements were made and averaged over 100 pulses.

The spatial characteristics of the resonator were studied using a Reticon 1024-G linear photodiode array and a RD-2 digitizer. The array has 1024 elements with a spacing between adjacent elements of 24.8 μm from center to center. Figures 11 and 12 are traces of the beam intensity profiles off the scraper in the unstable (horizontal) and stable (vertical) dimensions. The output appears to correspond to a Gaussian beam in the stable dimension and has diffractive structure in the unstable dimension. Figures 13 and 14 are traces of the beam intensity profile taken at M_1 in the stable and unstable dimensions.

Beam Quality Measurements

Pure astigmatism can be corrected by a cylindrical mirror or lens or by off-axis reflection from a spherical mirror. We wanted to determine the beam quality of the CBSUR if it were corrected for astigmatism. This was done by locating a slit at one of the two line foci corresponding to the stable and unstable directions. The fractional (peak) power passing through a vertical slit at the vertical line focus gave the beam quality in the unstable (horizontal) dimension. The fractional power passing through a horizontal slit at the location of the horizontal line focus gave the beam quality in the stable (vertical)

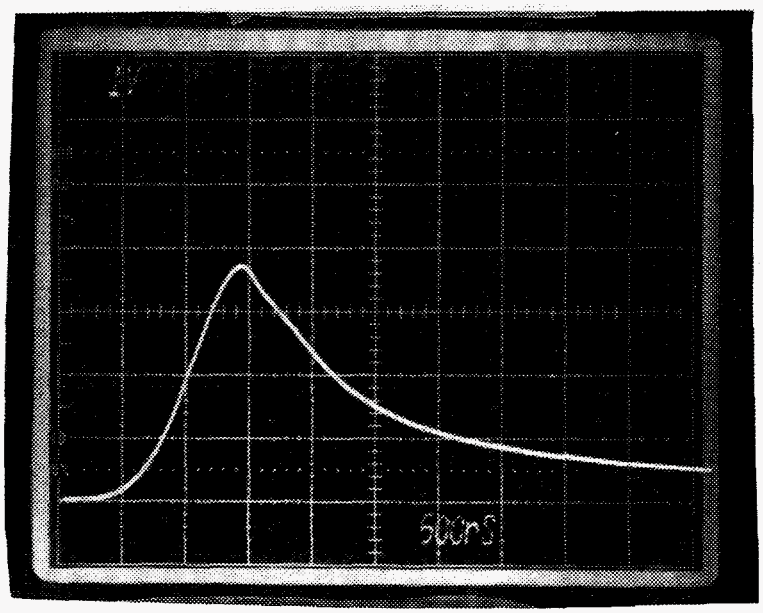

Figure 9. Sidelight fluorescence as a function of time. The trace is the output of a fast photodiode placed alongside the flashlamp and dye cell.

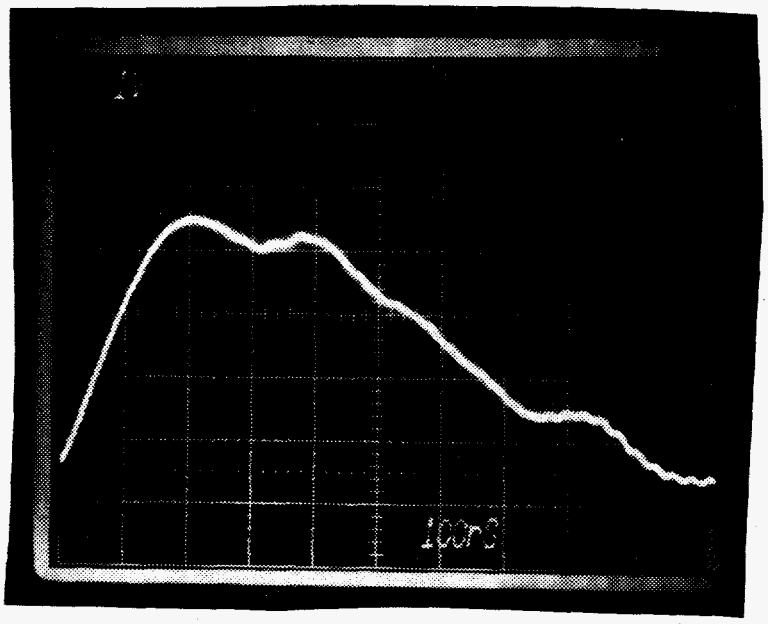

Figure 10. Laser power at Mirror M_1 as a function of time. A beamsplitter that reflected 9% of the incident power was placed in the resonator at M_1 and the output was focused onto a fast photodiode.

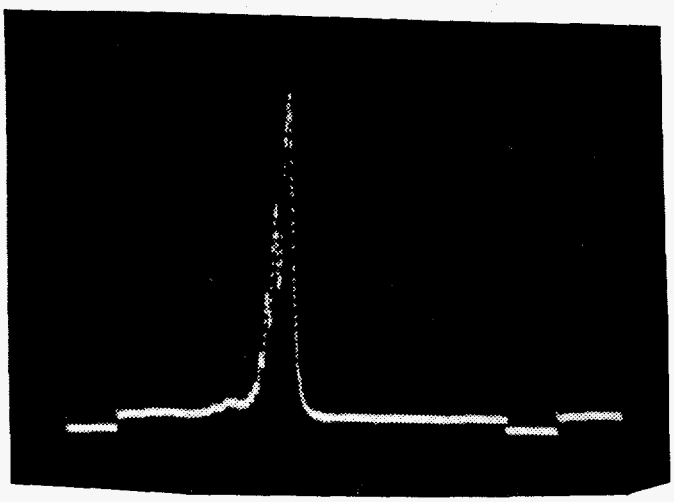

Figure 11. Beam intensity reflected from the scraper mirror as a function of x, showing the intensity profile in the unstable dimension. A horizontally oriented 1024-element photodiode array was placed 4" from the scraper.

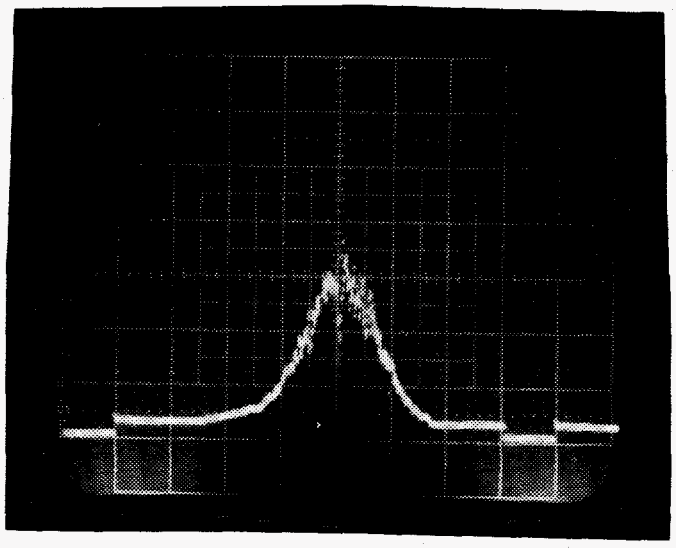

Figure 12. Beam intensity reflected from the scraper mirror as a function of y, showing the intensity profile in the stable dimension. A vertically oriented 1024-element photodiode array was placed 4" from the scraper.

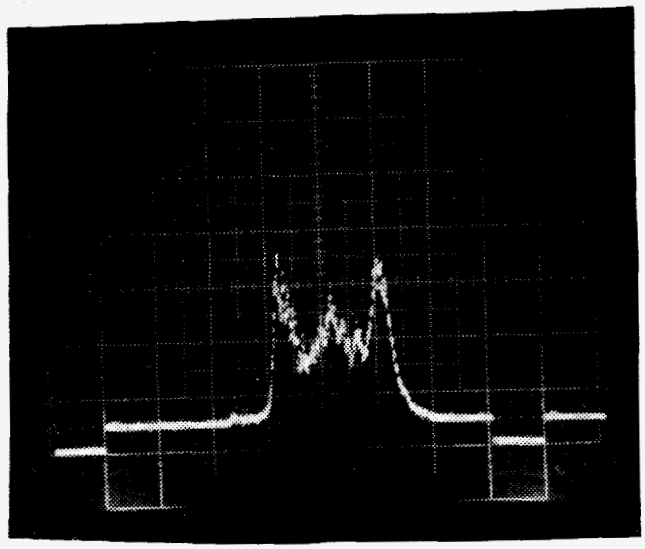

Figure 13. Beam intensity at Mirror M_1 as a function of x, showing the mode profile in the unstable dimension. A beamsplitter with a total reflectivity of 9% was placed 2" in front of M_1. The trace is the output from a 1024-element photodiode array placed 6" from the beamsplitter and oriented horizontally.

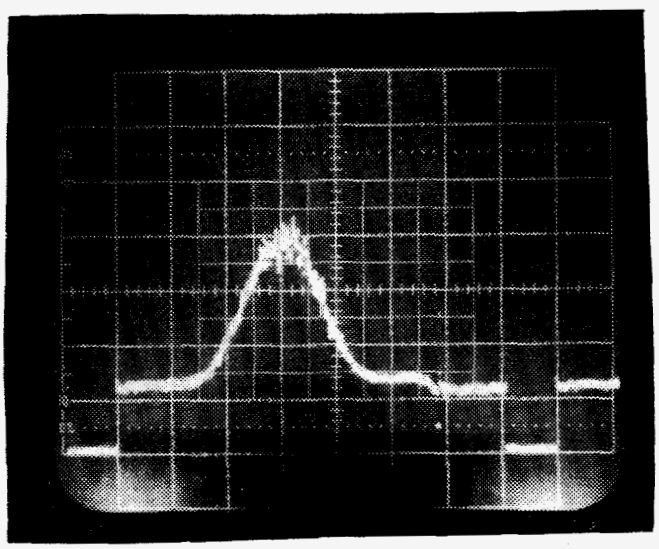

Figure 14. Beam intensity at Mirror M_1 as a function of y, showing the intensity profile in the stable dimension. A beamsplitter was placed 2" in front of M_1. The trace is the output from a 1024-element photodiode array placed 6" from the beamsplitter and oriented vertically.

dimension. The overall beam quality was the product of the values in the vertical and horizontal directions.

If the gain medium were not present, the beam in Region 2 of the resonator would be perfectly collimated in the vertical transverse dimension. The horizontal line focus would then occur at a distance of 300 cm from the focusing mirror. The focus of the beam in the unstable dimension would be closer to the focusing mirror. The gain medium had the effect of a positive lens, causing the beam to converge in both the horizontal and vertical transverse dimensions in Region 2. Each line focus was located by moving the reticon array along the beam until the best focus was found. The slit was placed at this location. The diagnostic layout we used for the beam-quality measurements is shown in Fig. 15.

Beam Quality in Unstable Dimension

The output from the resonator reflected from a mirror with a 3-meter focal length and came to a focus at a distance of 270.5 cm from its surface. The output beam from the laser had an irregular shape that made it difficult to directly measure its width, D_0 for use in beam quality measurements. We derived a geometric width of 0.301 cm. This was obtained by measuring the width of the resonator mode at mirror M_1 and correcting for the beam convergence in passing from the scraper mirror to M_1. The output beam width was obtained from the width of the feedback beam by substituting the nominal value of the magnification, $M = 1.357$, into the equation $D_0 = (M-1)\, D_{fb}$. The output beam converged with a radius of curvature of $R_u = 3051$ cm. This value was obtained from the location of the beam focus distance: $d = 270.5$ cm past the 3 m focusing mirror. The width of the output beam at the 3 m focusing mirror was $d = 0.272$ cm. A slit was placed at the focus and a photodiode was placed behind it. The (peak) power through the slit divided by the output (peak) power of the laser was measured for several values of the slit width. The data are plotted in Fig. 16 with a curve showing the integrated intensity that would result if a beam of width 0.272 cm with uniform intensity and parabolic wavefronts were brought to a focus at that location. The width of the central lobe for the ideal uniform-intensity beam is 0.117 cm. This would contain 0.903 of the power. The actual fraction of the power in this width, obtained by interpolating between grid points, was 0.846. The beam quality is the ratio of these, $n_u = 1.07$ in the unstable dimension.

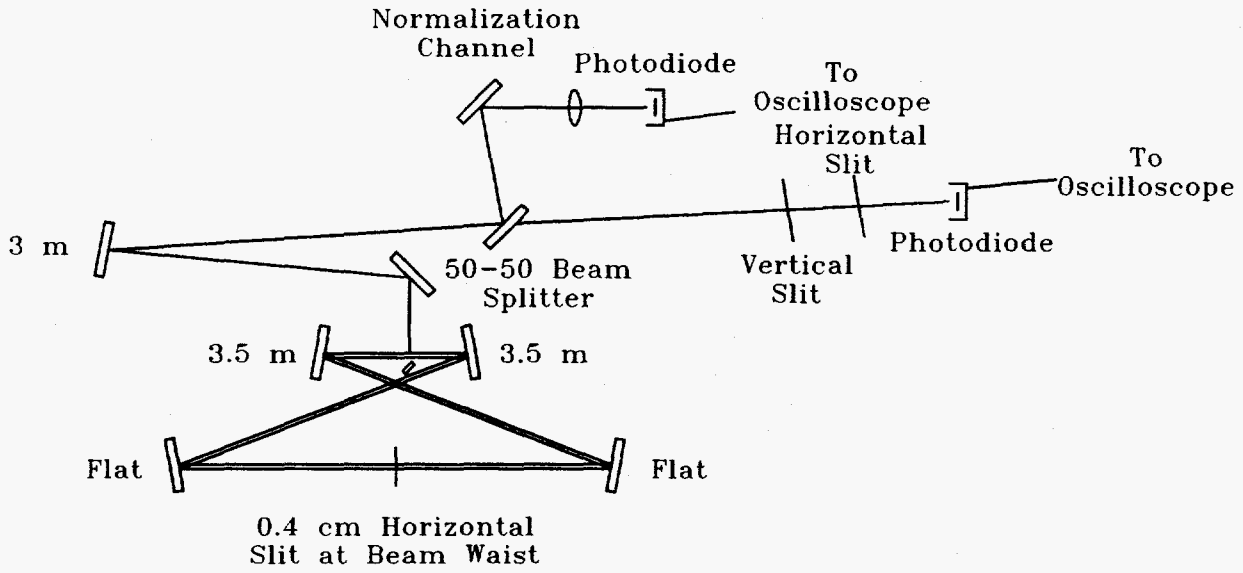

Figure 15. Diagnostic layout for beam-quality measurements. The horizontal slit for the measurement of the beam quality in the stable dimension was at 213.4 cm from the 3 m mirror. The vertical slit for the measurement of the beam quality in the unstable dimension was at 270.5 cm from the 3 m mirror.

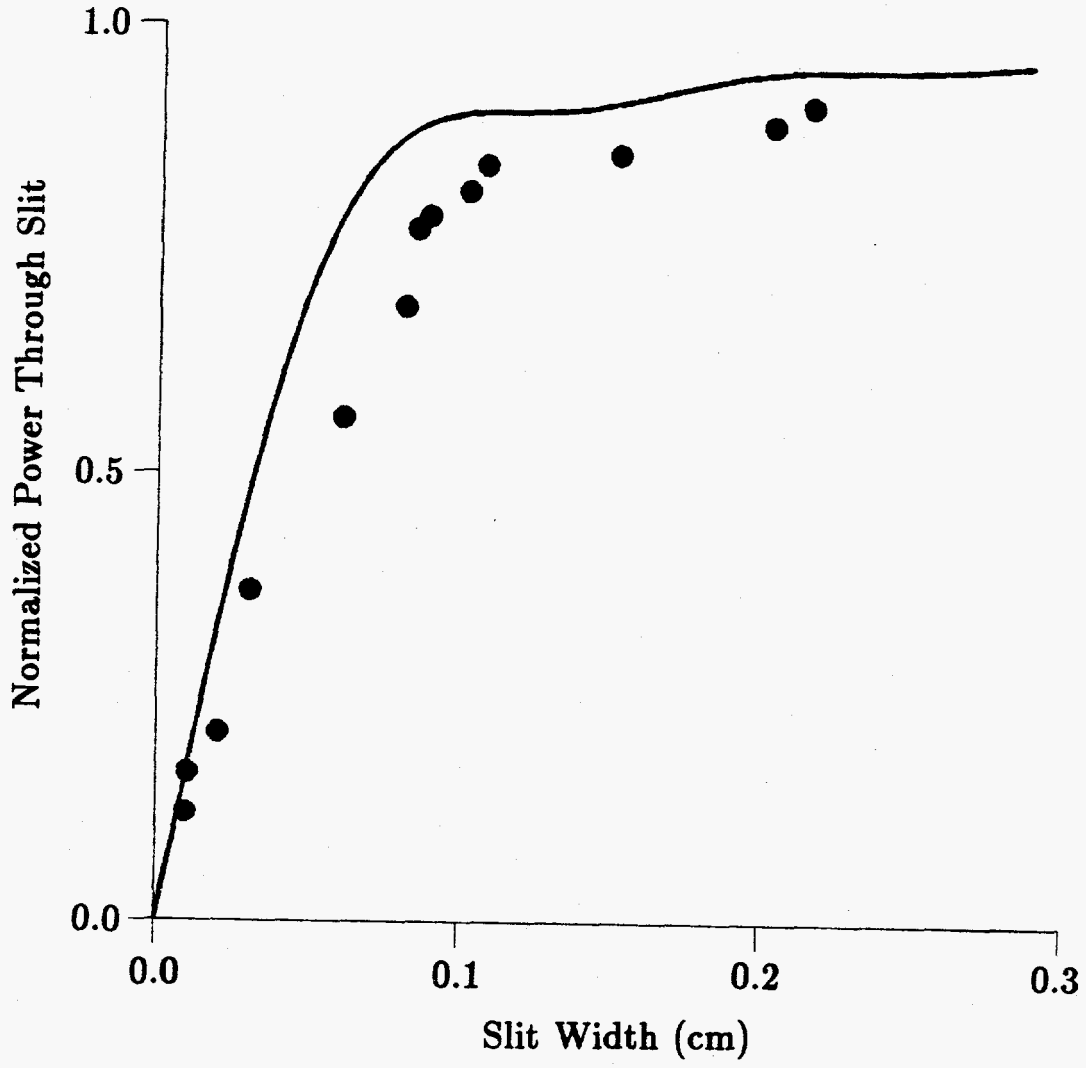

Figure 16. The plotted points give the fractional power through a vertical slit at the vertical line focus as a function of the slit width. The total output power was determined for each shot by splitting the output beam and measuring the total power in one branch. The curve gives the fractional power that would pass through the slit for an output beam with uniform intensity and ideal cylindrical wavefronts in the unstable dimension.

Beam Quality in the Stable Dimension

The focus in the stable dimension occurred at a distance of 213.4 cm from the 3 m mirror. This corresponds to a converging output beam with a radius of curvature of $R_s = 1038.8$ cm. The Gaussian-beam width at mirror M_1 was $w_1 = 0.49$ cm, which corresponds to a width of $w_3 = 0.363$ cm at the 3 m mirror. A horizontal slit was placed at the location of the focus with a photodiode behind it. The (peak) power through the slit was measured as a function of the slit width. The power through the slit was divided by the laser output power. The results are shown in Fig. 17. The solid curve shows the normalized integrated intensity for an ideal Gaussian beam with a width of 0.363 cm at the 3 m mirror. We define a beam quality in this dimension by selecting a slit width that would let 0.900 of the power pass for an ideal Gaussian beam. The width is 0.0182 cm. Interpolating between data points, we obtain a measured fraction of 0.80 of the incident energy through the slit. The beam quality is $n_s = 1.13$. The square of the overall beam quality is the product of the stable and unstable values, $n^2 = 1.21$, and the beam quality is $n = 1.10$.

Sensitivity to Mirror Tilt

Two slits were located 14 cm on either side of the beam waist in order to simulate the apertures at the ends of the wiggler magnets in a free-electron laser. The decrease in output (peak) power as a function of the tilt of mirrors M_1 and M_2 about horizontal axes was determined. Tilt that misaligns the mode in the stable dimension was studied because a free-electron laser would be more sensitive to tilt in this dimension due to clipping of the light beam at the end of the wiggler gap. Figure 18 shows the diagnostic layout for these measurements. Before the misalignment measurements, a set of data was taken to try to obtain an indication of the small-signal gain of the dye head. The horizontal edge of a plate was lowered into the beam in the expanded region to determine the decrease in output power as a function of the location of the edge of the plate. For all three sets of data, the voltage across the flashtubes was set to 18 kV, near the lowest value for which the laser would lase reliably in the aligned condition.

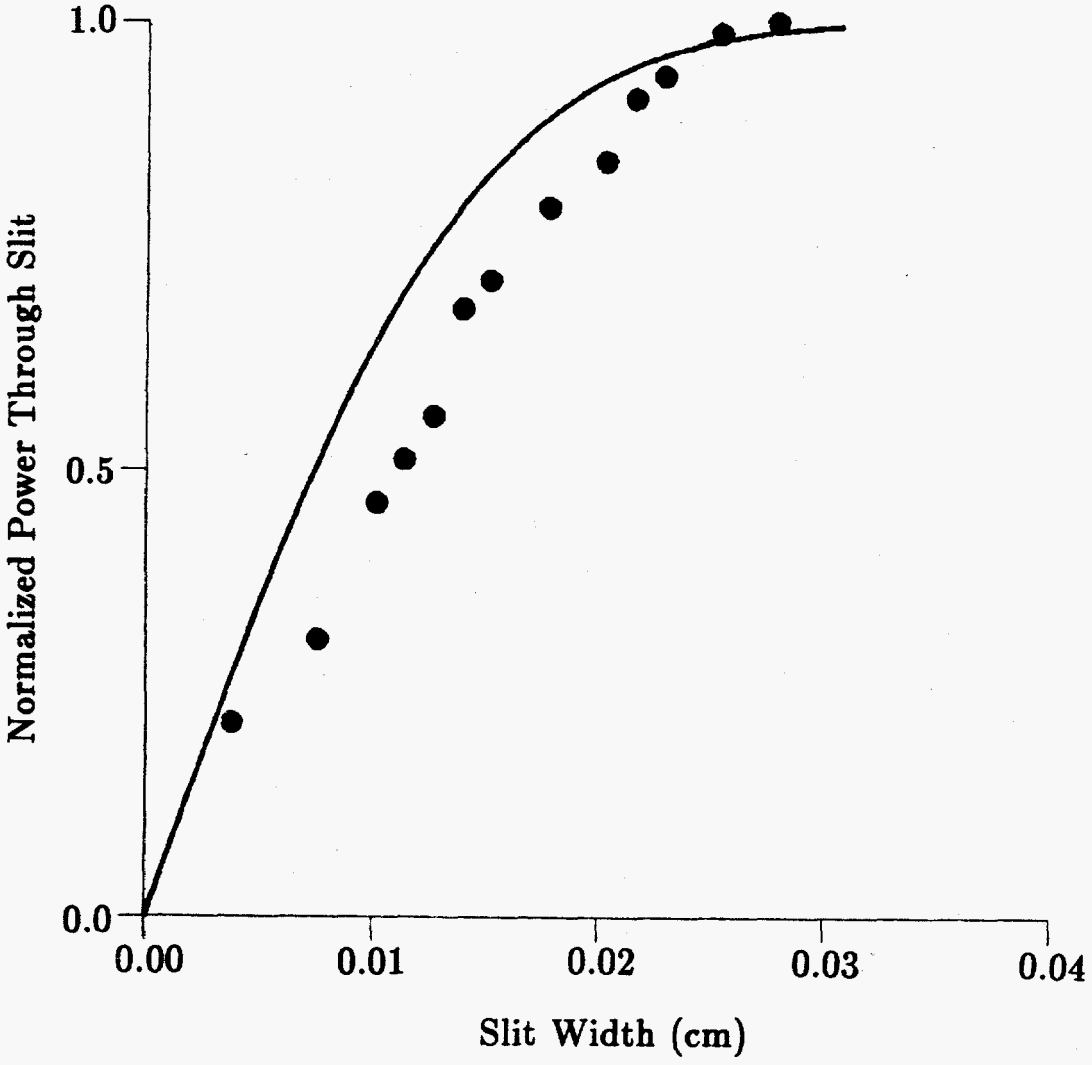

Figure 17. The plotted points give the fractional power through a horizontal slit at the horizontal line focus as a function of slit width. The curve gives the power that would pass through the slit for an ideal Gaussian beam.

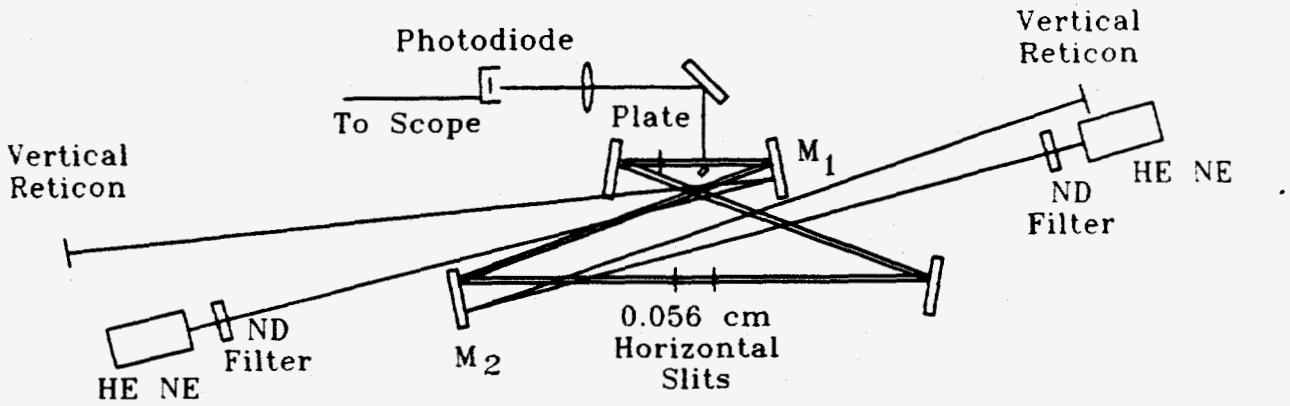

Figure 18. **Diagnostic layout for determining the sensitivity to mirror tilt. Two horizontal slits were symmetrically located 14 cm from the small beam waist. The beam from a HeNe laser was reflected from each mirror that was tilted and its position on a reticon array gave the tilt angle.**

The output power as a function of the distance from the bottom edge of the plate to the resonator optic axis is shown in Fig. 19. The optic axis location was obtained using a HeNe beam that was injected into the resonator and made to correspond to the optic axis during the alignment procedure. The resonator alignment was adjusted until the injected beam retraced its path after a round trip through the resonator. The heating of the dye during the laser pulse and the dependence of the index of refraction of the windows and dye on the wavelength may have resulted in a laser mode with a slightly different optic axis than that given by the HeNe beam. The points plotted on Fig. 19 are the experimental data. The solid and dashed curves were calculated using a laser simulation code. The product of the small-signal gain with the length of the dye tube, $g_0\ L_g$, is equal to 1.0 for the solid curve, and $g_0\ L_g = 2.0$ for the dashed curve. The sharp drop in the measured output power at 0.1 cm from the optic axis seems to favor the lower value for the gain. The laser simulation code is described in more detail below.

The measured output power as a function of the tilt angle of mirror M_1 is shown in Fig. 20. The solid and dashed curves were calculated using the laser simulation code with $g_0\ L_g = 1.0$ and 2.0, respectively. The computer model agrees with the experimental data very well, predicting values of the misalignment that are essentially the same as measured values corresponding to the same relative output power up to a tilt angle of about 17 μrad.

The simulated and measured values of the output power as a function of the tilt of mirror M_2 are shown in Fig. 21. The angle corresponding to a given loss is much larger than for mirror M_1. The simulated curves agree reasonably well with the measured values, but give a tolerance that is somewhat larger for a given power loss.

Computer Simulation of Experimental Laser

A strip-resonator code was used to simulate the laser with misalignment in the vertical direction. The stable transverse dimension was simulated using a diffractive code, and the outcoupling was included by normalizing the field to reduce the circulating power to a factor of 0.73 of the incident power at the location of the outcoupling mirror. A simple

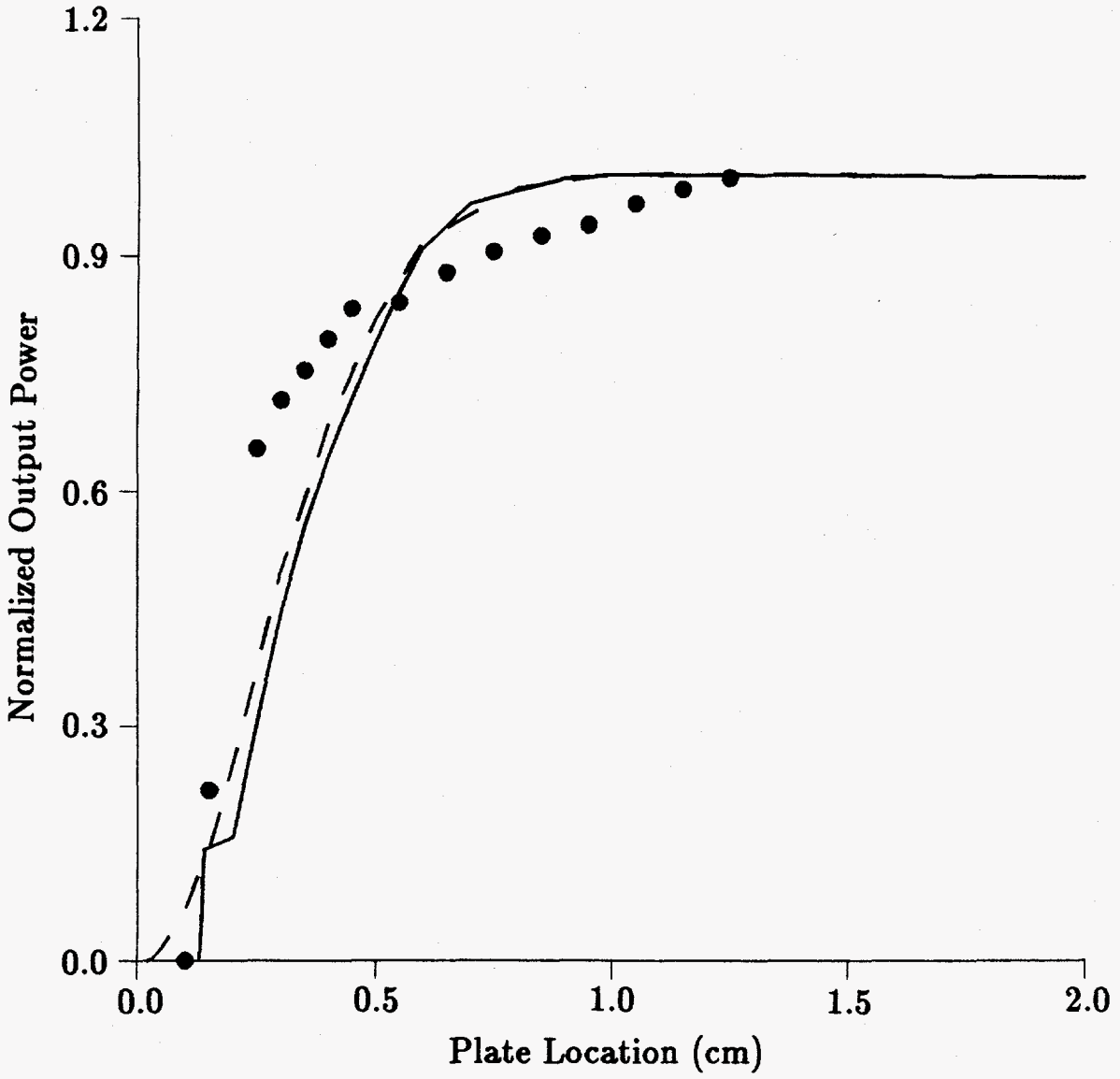

Figure 19. Fractional output power as a function of the location of the horizontal edge of a plate that was lowered into the laser beam in Region 2. The points give the experimental data and the curves were calculated using a diffractive computer code. The solid and dashed curves correspond to $g_0 L_g = 1.0$, and $g_0 L_g = 2.0$, respectively.

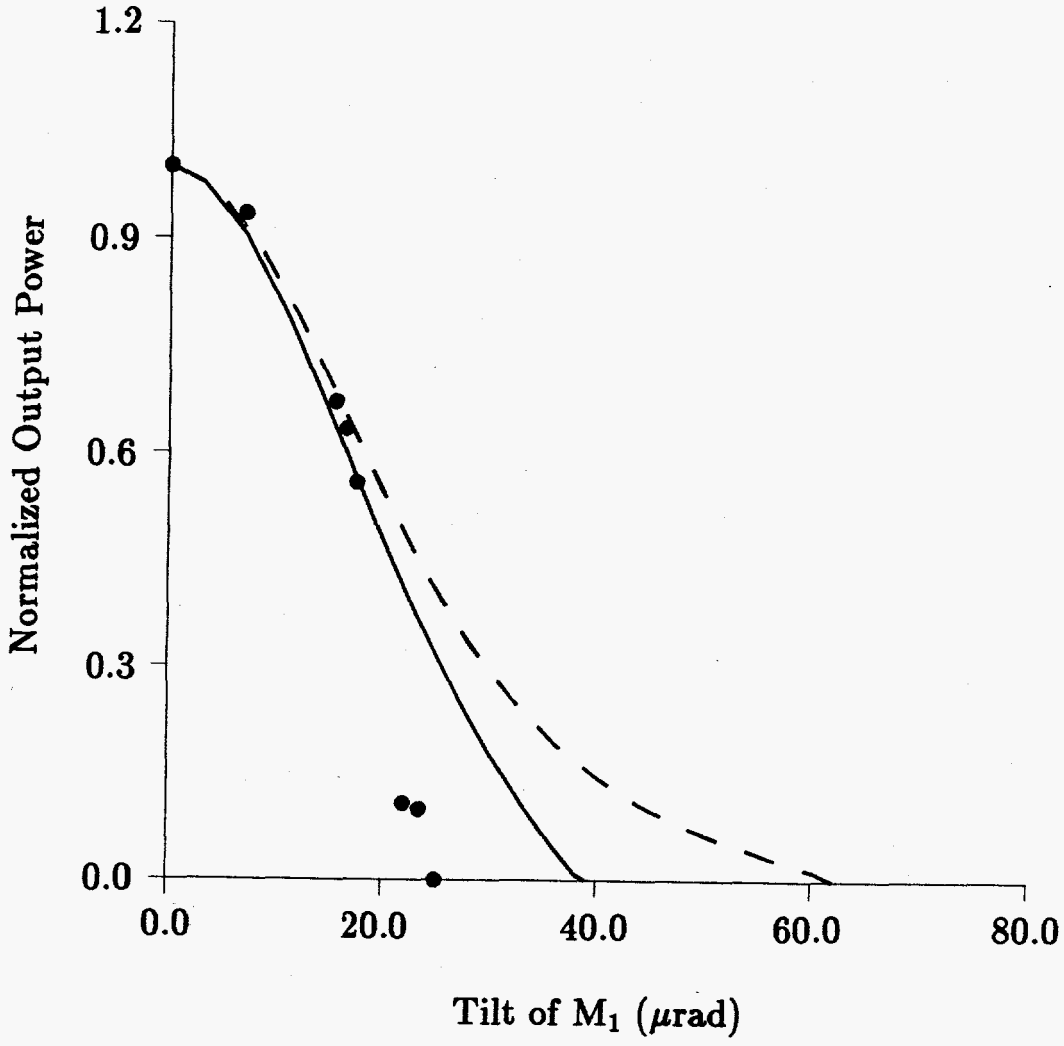

Figure 20. Fractional output power as a function of the tilt angle of Mirror M_1. The points give the experimental data and the curves were calculated using a diffractive computer code. The solid and dashed curves correspond to $g_0 L_g = 1.0$, and $g_0 L_g = 2.0$, respectively.

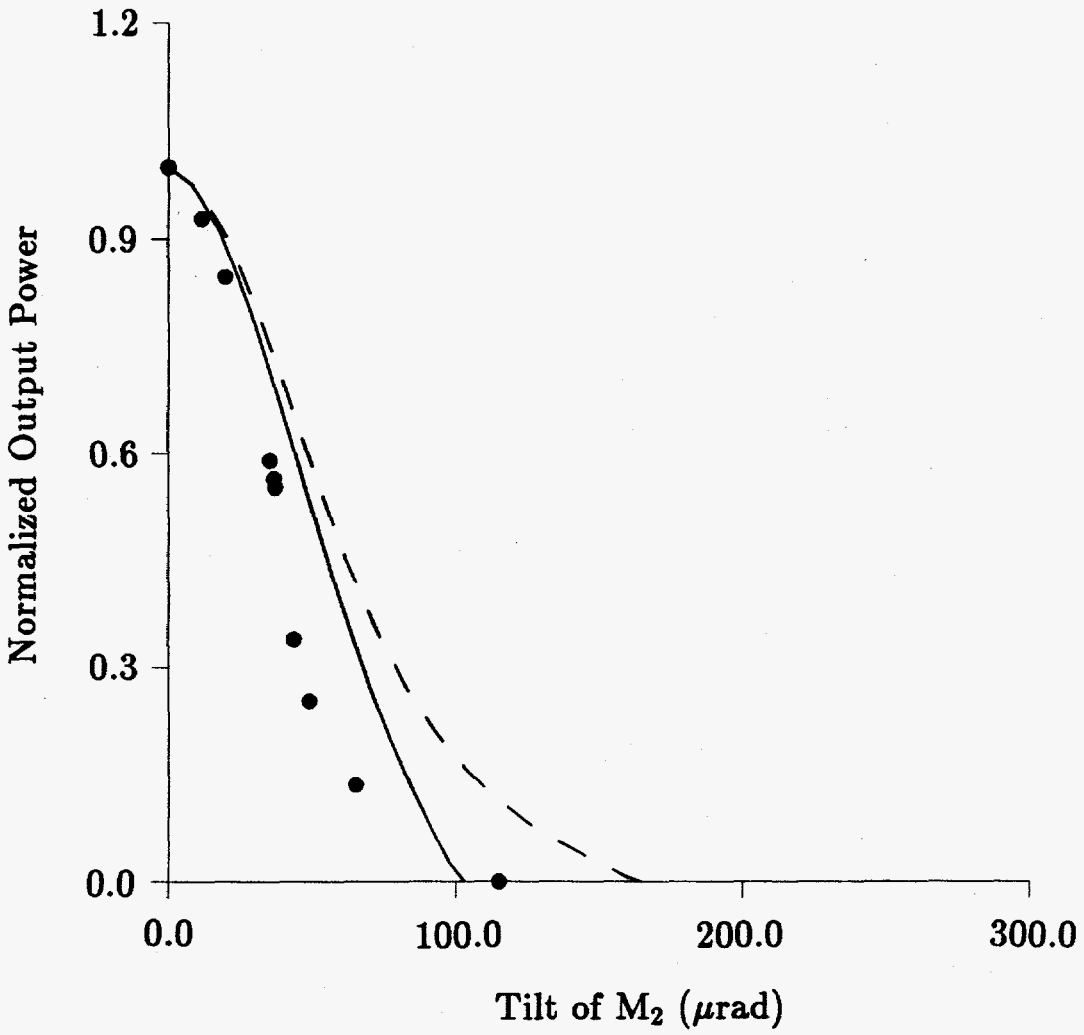

Figure 21. Fractional output power as a function of the tilt angle of Mirror M_2. The points give the experimental data and the curves were calculated using a diffractive computer code. The solid and dashed curves correspond to $g_0 L_g = 1.0$, and $g_0 L_g = 2.0$, respectively.

saturable gain algorithm was included to represent the dye laser head, and the gain was lumped at a single transverse sheet at its center.

To check the diffractive propagation code, we calculated the size of the beam at one of the spherical mirrors and at the small waist of a ring resonator that was not as close to the boundary of stability as the nearly confocal resonator that is the subject of this report. Our reason for selecting a different resonator was that the mode of a resonator that is near the boundary of stability is changed significantly by the finite apertures that must be included in a diffractive calculation (and in a real laser). The correct answer for the diffractive code would not necessarily agree with the ideal aperture-free Gaussian-beam theory. The results for a ring resonator with $L_1 = 660$ cm, L_2=400 cm and mirror focal length $f_1 = f_4 = 400$ cm were compared with the values obtained from the Gaussian-beam equations discussed above. The waist size calculated using Gaussian-beam theory was 0.8127 mm, and the value obtained from the bare-cavity diffractive code was 0.8148 mm. The beam size at the mirror was 1.438 mm using Gaussian-beam theory and 1.444 mm using the diffractive code, which is very good agreement. The number of grid points used in this comparison was 256.

The propagation algorithm used in the code was the kernel-averaged fast Fourier transform algorithm developed by Phelps.[18,19] In our experience, accurate answers can be obtained for problems in which the field is clipped near a focus with fewer grid points than are required using the more conventional algorithm of Sziklas and Siegman.[20] An expanding coordinate system[16,20] was used to match the size of the calculational grid to the size of the beam at planes where the field was evaluated. The number of grid points used in the calculations was 1024.

Modified configuration with the unstable focus at the location of the stable waist

The resonator shown in Figs. 1 and 2 is adequate to compare theory and calculations with the performance of the compact-beam stable-unstable resonator, but it would probably not be desirable to use a scaled version of this exact configuration in a FEL. The problem is, the intracavity focus of rays in the tangential plane (unstable dimension) does not occur at the same location as the focus of rays in the saggital plane (stable

dimension). Many modifications are possible to correct this situation. A negative cylindrical mirror oriented so that it causes additional divergence of rays in the tangential plane can be substituted for mirror M_3 of Fig. 1. The modified resonator is sketched in Fig. 22. The focal length of the cylindrical mirror is selected so that the intracavity focus occurs at the center of Region 1. For our initial configuration, the focal length required to move the focus to the center of section L_{1b} is $f_3 = -758.6$ cm. However, the magnification is reduced to $M = -1.156$. The magnification can be made larger by increasing the angle of incidence of the beam at each of the spherical mirrors. For example, an increase from 10° to 15° requires the lengthening of region L_1 from 710.000 cm to 723.895 cm to keep $2f_s$-L_1 the same so that the stable mode waist size is essentially the same as for the initial resonator. If we select $L_{1c} = L_{1a} = 220.0$ cm giving $L_2 = 97.2$ cm, a magnification of $M = -1.31$ results, and the focal length required for the cylindrical mirror replacing M_3 is $f_3 = -304.1$ cm. Configurations with higher magnification are possible by further increasing the angle of incidence at the spherical mirrors.

The equations for the centers of curvatures of the mode are simpler than than the corresponding equations not including the cylindrical mirror, Eqs. 8-10.

Only linear equations result because the location of the intracavity focus is known initially. Let d_1 be the distance from mirror M_4 to the center of curvature of the beam in Region 1c; a positive value corresponds to an expanding beam. Let d_2 be the distance from mirror M_4 to the center of curvature of the beam in Region 2; a positive value corresponds to an expanding beam. Also, define h = 0.5 L_1. The equation for d_2 is

$$\frac{1}{L_2 + d_2} + \frac{1}{h} = \frac{1}{f_t} \tag{18}$$

and d_1 is obtained from

$$\frac{1}{d_1} - \frac{1}{d_2} = \frac{1}{f_t} \tag{19}$$

and the equation for f_3 is

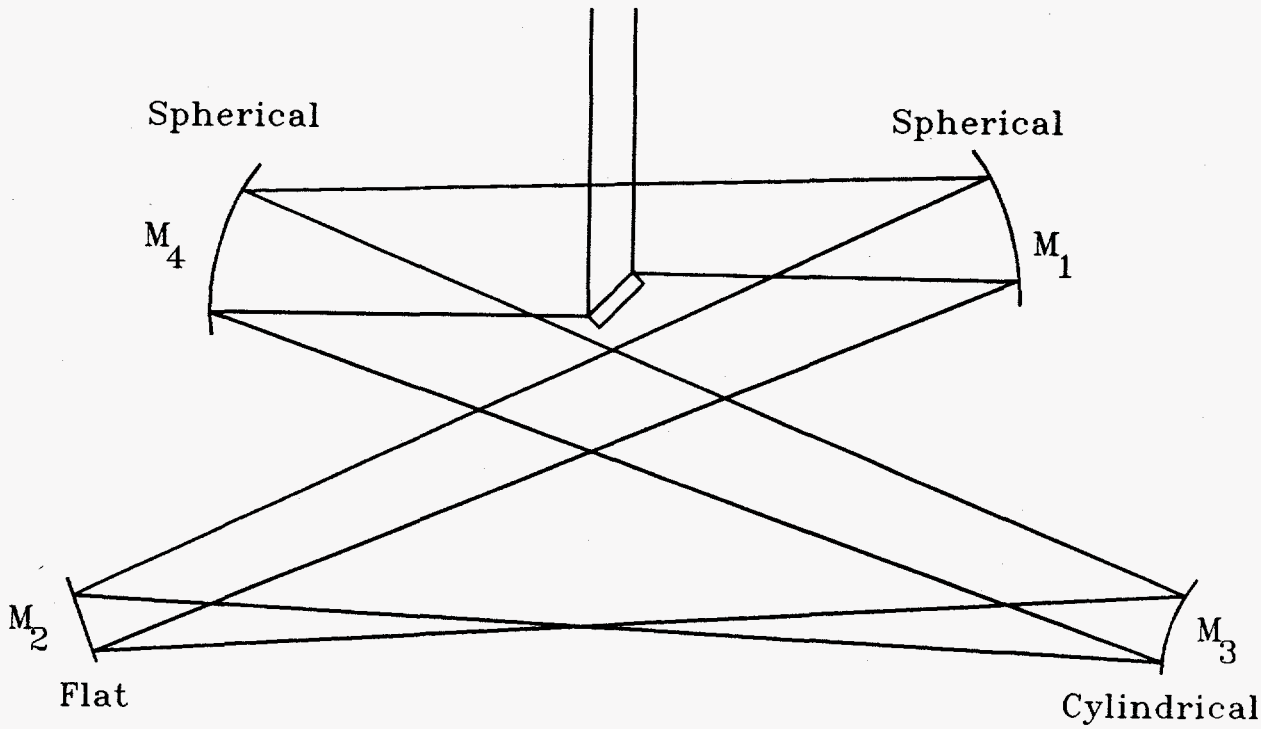

Figure 22. Resonator configuration similar to the experimental setup, but with a cylindrical mirror substituted for a flat to move the intracavity focus in the tangential plane to the location of the Gaussian beam waist in the saggital plane.

$$\frac{1}{f_3} = \frac{1}{L_{1c} - d_1} + \frac{1}{h - L_{1c}} \tag{20}$$

These equations were obtained by imaging the center of curvature of a segment of the mode through the intervening optical element to obtain the center of curvature of the next segment. The resonator magnification is the product of the individual values for the segments,

$$M = -\left(\frac{h - L_{1c}}{h}\right)\left(\frac{L_2 + d_2}{L_2}\right)\left(\frac{d_1}{d_1 - L_{1c}}\right) \tag{21}$$

Other resonator configurations with the tangential intracavity focus occuring at the saggital beam waist are possible. A configuration involving two extra mirrors is sketched in Fig. 23. This configuration has the advantage that the output beam would not have to be corrected for astigmatism. The angle of incidence is adjusted so that in the saggital plane, the spherical mirrors are almost confocal, at a point centered between the two flat mirrors. In this dimension they both have effective focal length f_s that is slightly too large for them to be confocal. In the tangential plane, shown in Fig. 23, the spherical mirrors are exactly confocal (using the effective focal length) at the point halfway between the two flat mirrors. The cylindrical mirrors form a confocal telescope. Then the output beam is collimated and has no astigmatism (assuming that the Gaussian beam width in the saggital planes at the spherical mirrors is much larger than the small beam waist).

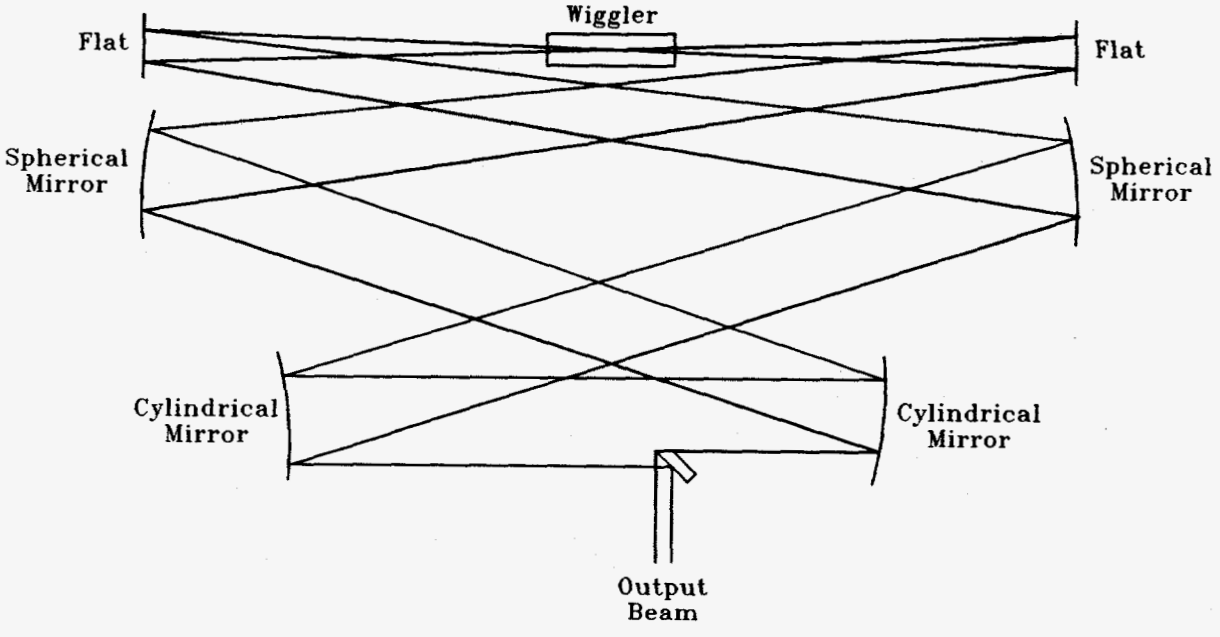

Figure 23. Version of the CBSUR with a cylindrical telescope in the expanded segment.

2.0 REFERENCES

1. R. L. Tokar, B. D. McVey, and J. C. Goldstein, *"Sideband Suppression in Free-Electron Lasers Using a Grating Rhomb,"* IEEE J. Quantum Electron., Vol. 24, pp. 856-863, 1988.

2. G. T. Moore, *"Unstable Resonators for the Free-Electron Laser,"* Proc. SPIE , *"Free Electron Generators of Coherent Radiation,"* C. A. Brau, S. F. Jacobs, and M. O. Sculley, Eds., Vol. 453, pp. 255-260, 1984.

3. A. H. Paxton, *"Unstable Resonators with Negative Equivalent Fresnel Numbers,"* Opt. Lett. Vol. 11, pp.76-78, 1986.

4. E. Sklar, *"The Advantages of a Negative-Branch Unstable Resonator for Use with Free-Electron Lasers,"* IEEE J. Quantum Electron. Vol. QE-22, pp. 1088-1094, 1986.

5. P. K. Kennedy, K. C. Sun, R. H. Labbe, and R. A. Cover, *"Effect of Various Outcoupling Options on Free-Electron Ring Laser Performance,"* IEEE J. Quantum Electron, Vol. 25, pp. 2322-2326, 1989.

6. R. W. Jones and J. F. Perkins, *"Transverse Mode Properties of Beam-Rotated Unstable Resonators for Free Electron Lasers,"* J. AIAA, Vol. 26, pp. 897-900, 1988.

7. M. J. Schmitt and A. H. Paxton, *"Free-Electron Lasers Using Stable-Unstable Ring Resonator,"* SPIE , Symp. Lasers and Opt., Jan. 15-20, 1989, Vol. 1045, pp. 36-43.

8. R. K. Luneburg, Mathematical Theory of Optics. Berkeley, CA: University of California Press, 1964, p.234.

9. O. L. Bourne and P. D. Dyer, *"A Novel Stable-Unstable Resonator for Beam Control of Rare Gas Halide Lasers,"* Optics Commun. Vol. 31, pp 193-196, 1979.

10. A. Borghese, R. Canevari, V. Donati, and L. Garifo, *"Unstable-Stable Resonators with Toroidal Mirrors,"* Applied Opt. Vol. 20, pp. 3547-3552, 1981.

11. R. W. Jones, C. Cason, and J. F. Perkins, *"New Laser Resonator with Unobscured Reflective Outcoupling and Internal Optic Axis,"* presented at AIAA 19th Fluid Dynamics, Plasma Dynamics, Lasers Conf., Honolulu, HI, June 8-10, 1987.

12. A. E. Siegman, Presented at Conf. on Lasers and Electro-Optics, Baltimore, MD, May 14-16, 1991.

13. A. H. Paxton and W. P. Latham, Jr., *"Ray Matrix Method for the Analysis of Resonators with Image Rotation,"* SPIE, International Lens Design Conf., Vol. 554, pp.159-163, 1985.

14. A. H. Paxton and W. P. Latham, Jr., *"Unstable Resonators with 90° Beam Rotation,"* Applied Opt., Vol. 25, pp. 2939-2946, 1986.

15. J. M. Eggleston, *"Angularly Stable Ring Resonators for High Power FEL's. in Proc. Int. Conf. Lasers '83,"* Dec. 12-16, R. C. Powell, Ed. Mclean,VA:STS Press, 1983, pp. 305-310.

16. A. E. Siegman, Lasers, Mill Valley, CA: University Science Press, 1986.

17. Yu. A. Anan'ev, *"Unstable Resonators and their Applications,"* Sov J. Quantum Electron., Vol. 1, pp.565-586, 1972.

18. The propagation algorithm was devised by D. Phelps, AFWL-TR-74-344, 1974, p.80.

19. The propagation algorithm devised by D. Phelps is outlined in P. W. Milonni and A. H. Paxton, *"Model for the Unstable-Resonator Carbon Monoxide Electric-Discharge Laser,"* J. Appl. Phys., Vol. 49, pp. 1012-1027, 1978.

20. E. A. Sziklas and A. E. Siegman, *"Mode Calculations in Unstable Resonators with Flowing Saturable Gain. 2: Fast Fourier Transform Method,"* Appl. Opt. Vol. 14, pp. 1874-1889, 1975.

APPENDIX A

REPRINTS OF TWO PAPERS

M.J. Schmitt and A.H. Paxton, "Free Electron Lasers Using Stable-Unstable Ring Resonators," in Modeling and Simulation of Laser Systems, Donald L. Bullock, Editor, SPIE Proceedings, Vol. 1045, pp. 36–44, 17–18 January 1989.

A.H. Paxton and M.J. Schmitt, "Sideband Instability in Free-Electron Lasers – A New Technique for Suppression," IEEE J. Quantum Electron; Vol. 26, pp. 1167–1172, 1990.

Free Electron Lasers using Stable-Unstable Ring Resonators

Mark J. Schmitt and Alan H. Paxton

Mission Research Corporation, 127 Eastgate Drive, Suite 208
Los Alamos, New Mexico 87544

ABSTRACT

The free electron laser (FEL) simulation code FELEX is used to examine the operation of stable-unstable FEL resonators. These resonators are stable along one transverse axis and unstable along the orthogonal transverse axis. The simulations utilize a ring resonator with an intracavity focus in the unstable plane near the center of the wiggler (close to the same axial position as the waist in the stable plane) thereby enhancing the coupling between the optical and electron beams. Asymmetric output scraping is performed in the back leg of the ring using a reflective mirror inserted from one side of the unstable axis. Resonators with relatively low equivalent Fresnel number ($|N_{eq}| \leq 10$) and magnification ($|M_x| \simeq 1.2$) are examined. Optical characteristics including the cavity mode profile at various positions inside the resonator are shown.

1. INTRODUCTION

The construction of laser oscillators with very high circulating powers requires the use of totally reflective optical elements. Such elements minimize the absorption of optical power and allow for mirror substrate cooling across the entire mirror aperture. Stable resonators employing these optical elements can only be out-coupled using either diffractive elements[1], halo scrapers or hole couplers. Unfortunately, each of these techniques suffers from at least one drawback. Diffraction gratings of significant size are difficult to fabricate and have significant losses; halo scrapers produce annular output beams that have inferior focus intensities and hole couplers produce a loss of on-axis intracavity intensity that reduces laser efficiency. One can avoid the use of these techniques by allowing the cavity geometry along one transverse axis to become unstable, such that an output coupling scheme previously described [2-5] can be employed. This scheme involves asymmetrically scraping one edge of the ciculating optical beam as shown in Figure 1. The position of the scraper edge dictates the size of the optical mode along the unstable axis. Since the cavity has a focus in the unstable plane, output scraping of only one side of the optical beam is required to limit the mode size at both edges. This is a consequence of the field inversion that occurs at the focus. Thus, each edge of the mode is scraped on every other pass through the cavity. This output coupling scheme also has the advantage that a filled-in output beam is produced which propagates to a central peak in the far field.

A study has been undertaken to examine the properties of this type of resonator for free electron laser applications. The three-dimensional code FELEX[6] is being used to model both the optical propagation in the resonator and the interaction of the optical mode with the electron beam inside the wiggler. In Section 2 initial simulations are compared to previously published unstable cavity mode profiles for code validation purposes. These simulations include linear and ring geometries with and without intracavity foci. Simulation of the cavity of a stable-unstable dye laser currently in operation is conducted in Section 3. Subsequent simulations of the stable-unstable resonator with a FEL as the active gain medium are given in Section 4.

2. BARE-CAVITY SIMULATIONS

Prior to this work, FELEX was primarily used to investigate the operation of FELs employing stable resonators. One primary difference between stable and unstable resonator simulations is the high transverse spatial frequencies introduced by aperturing (or scraping) in the unstable direction. Owing to the discrete nature of the simulation, the discontinuity in the optical field imposed by these apertures can give rise to aliasing of the field at subsequent propagation locations. The following three techniques were used to control these high spatial frequency components.

- Aperture Apodization: the transmission (T) of the optical field near the edge of hard apertures was changed from a step function to a smoothly varying sinusoidal function of the form

$$T = \frac{1}{2}\left\{1 + \sin\left[\frac{\pi}{2}\frac{x - x_{ap}}{h_{ap}}\right]\right\} \qquad |x - x_{ap}| \leq h_{ap} \tag{1}$$

where x_{ap} is the location of the aperture edge and h_{ap} is the half-width of the apodization region. The half-width is specified by an integer number of grid points and was typically 2 to 4 depending on the grid resolution. Although the field values on the grid are a piecewise approximation of the expression in Eq.(1), significant reductions in aliasing can be achieved with apodization over just a few grid points. Care was taken to keep the half-width of the apodization region small enough so that the physics of the problem being studied was not altered. The cavity mode would be significantly changed if the deviation in the radius of the aperture introduced by the apodization modified the equivalent Fresnel number of the resonator by unity. Therefore, the half-width of the apodization was chosen to keep $\Delta N_{eq} \ll 1$.

- Spatial Frequency Filtering: The algorithm used to propagate the optical field in free-space involves the use of fast Fourier transforms (FFT). In transform space the large wavenumber values will appear at the edges of the 2-D field array. These large wavenumber field components can be suppressed by applying an apodized "wavenumber aperture" to the electric field transform array. In FELEX this filter has the form

$$T_k = \frac{1}{2}\left\{1 - \cos\left[\pi\frac{k/k_{max} - k_{ap}/k_{max}}{1 - k_{ap}/k_{max}}\right]\right\} \tag{2}$$

where k_{max} is the maximum wavenumber allowed by the grid such that k_{ap}/k_{max} is the normalized input wavenumber specifying where the filtering begins. As with the spatial apodizer, one must take care not to change the problem by excessively filtering in Fourier space. A reasonable guideline for the truncation of spatial frequencies is given by

$$\lambda_{min} \leq \frac{\text{Fresnel zone}}{5} \tag{3}$$

where λ_{min} is the shortest transverse wavelength remaining after filtering. When employed, this filtering procedure is performed at each propagation step through the resonator.

- Aperturing at a Focus: Since the optical field profile at a focus is just a scaled version of the Fourier transform of the electric field, one can filter out the high frequency spatial components by introducing an aperture at the focus that scrapes off the wings of the field. The application of this technique differs from the above case in that the truncation of the higher spatial frequencies is imposed more abruptly and at only specific positions in the resonator.

Cavities with low equivalent Fresnel numbers were modeled using one or more of the previously described filtering techniques to control aliasing. Low Fresnel number cavities were chosen to minimize the amount of transverse resolution required to adequately resolve the problem. A transverse grid of 128×128 was commonly used. The propagation algorithm used an expanding grid coordinate system, similar to that described by Sziklas and Siegman[7]. The size of the grid was initially set equal to 2.5 times the geometric size of the beam in the resonator. When modeling resonators with symmetric scrapers, an interpolator was used to magnify the remaining field, thereby maintaining optimum resolution.

As an initial test case, a symmetric standing-wave resonator with $M = 1.42$ and $N_{eq} = .52$ was chosen. The mode profile obtained was in close agreement with that given by Rensch and Chester[8].

Next, an attempt to model a confocal ring resonator with $M = -1.42$, and $N_{eq} = -3.12$ was made. The ring configuration is shown in Figure 2. Note that the ring incorporates transmissive optics while an actual high-power resonator would employ cylindrical or spherical mirrors. Although the ring has a negative magnification and equivalent Fresnel number (owing to the intracavity focus), the mode pattern at the output scraper will be identical to the mode pattern on either mirror of a positive branch symmetric resonator if the magnitudes of M and N_{eq} for the two resonators are identical. To calculate the Fresnel number of the ring

we use the property[9] that the reciprocal of the cavity Fresnel number is equal to the sum of the reciprocal Fresnel numbers of the individual segments of the cavity. With the help of Figure 2, the collimated Fresnel number of the ring can be expressed

$$N_c^{-1} = \frac{\lambda}{a^2}\left[L_1 - \frac{L_2}{M} + \frac{L_3}{M^2}\right] \tag{4}$$

where a is the aperture half-width. Using this relation in conjunction with the expression for N_{eq} given by

$$N_{eq} = \frac{M^2 - 1}{2M^2} N_c \tag{4}$$

the various cavity lengths can be chosen to obtain the desired M and N_{eq}.

Initial simulations produced mode patterns that deviated significantly from those given by Rensch and Chester[8]. However, by placing an aperture at the intracavity focus, an intensity profile closely resembling the pattern given in [8] was achieved. Figure 3a and 3b show the mode pattern from [8] and from the FELEX simulation with focal aperturing. Since the exact filtering algorithm used in [8] was not specified by the authors, a closer comparison could not be performed. An additional comparison was made of the mode pattern obtained analytically by Rodgers and Erkkila[10]. They conducted calculations for a standing-wave resonator with $M = 2.5$ and $N_{eq} = 3.12$. This resonator was modeled again using a negative branch ring configuration with the same parameter magnitudes. To control aliasing, apodization over 4 grid points was employed and an aperture was placed at the focus. The lowest order mode pattern from their paper is given in Figure 4a while the simulation result is given in Figure 4b. The results of these comparisons indicated that the FFT propagator in FELEX was adequate for modeling unstable resonator geometries.

3. EXPERIMENTAL COMPARISON

A stable-unstable ring laser has been constructed at MRC-Albuquerque. The resonator has near confocal geometry with astigmatism introduced to make the ring unstable in one dimension. The magnification of the cavity was kept low ($|M| \simeq 1.2$) to limit the the output coupling. This keeps the saturated single-pass gain in the FEL simulation relatively low ($10 \simeq 30\%$). As a result, the amount of mode distortion[11] caused by the gain in the narrow electron beam will not significantly alter the mode shape of the bare-cavity resonator. In the experiment a laser dye tube provided the active gain media.

The equivalent resonator depicted in Figure 5 was used to model the experimental resonator. The simulation converged after approximately 20 passes to a loss of $\simeq 14\%$ per pass. Transverse profiles in the unstable direction of the experimental mode and the mode from the simulation are shown in Figure 6. Clean gaussian mode profiles were obtained in the orthogonal transverse plane both experimentally and in the simulation.

4. STABLE-UNSTABLE FEL SIMULATIONS

A modification of the propagation algorithm had to be made before the FEL interaction could be included in the simulation model. FELEX uses a fixed (non-expanding) grid inside the wiggler. A finite difference algorithm is used in this region so that the optical source due to the electrons can be added in as the optical field is stepped through the wiggler. As a final check, the finite difference propagator was tried through the wiggler region with no electron beam present. The results obtained were identical to the previous simulations using only the FFT propagator.

A scaled (with identical M and N_{eq}) version of the experimental stable-unstable ring analyzed in Section 3 was modeled. The cavity dimensions were increased so that the Rayleigh range was equal to the length of typical experimental wigglers ($\simeq$ 1 meter). Approximately 20 passes were required for the optical mode to converge in the unstable direction. Then, depending on the amplitude of the initial optical field, the circulating power in the cavity increased until saturation was reached. A 3-D plot of the transverse electric

field at the end of the wiggler is given in Figure 7. The mode in the unstable direction has several side lobes (caused by the high transverse spatial frequencies) while the mode in the stable direction has a narrow gaussian dependence. The size of the optical mode was chosen so that the central lobe of the optical mode was approximately twice the size of the electron beam. This assured that virtually all the electrons interacted efficiently.

The output beam scraped off one side of the unstable direction in the back leg of the resonator is shown in Figure 8a. Since the beam is unobscured, it can be focused to a narrow spot as shown in Figure 8b. This focusing ability is crucial for applications where high intensity is desired.

5. CONCLUSIONS

We have shown that FELEX is an effective tool for addressing the usefulness of stable-unstable resonators for free electron laser applications. Good agreement has been obtained both with previously published unstable mode profiles and with the experimentally measured mode profiles of the stable-unstable laser currently operating at Mission Research Corporation in Albuquerque. The simulations show that a clean output beam can be obtained using an asymmetric scraper in conjunction with the stable-unstable FEL cavity configuration. More simulations will be required to determine the operating characteristics of such resonators for high power applications.

6. ACKNOWLEDGMENTS

The authors would like to thank Dr. B. D. McVey of Los Alamos National Laboratory for his helpful suggestions concerning the operation of FELEX. This work supported by the Strategic Defense Initiative Organization.

7. REFERENCES

1. R. L. Tokar, B. D. McVey and J. C. Goldstein, "Sideband suppression in free electron Lasers using a grating rhomb", IEEE J. Quantum Electronics, June, (1988).
2. Edward Sklar, "The advantages of a negative branch unstable resonator for use with free-electron lasers", IEEE J. Quantum Electronics, QE-22, 1088-1094, (1986).
3. Edward Sklar, "The tilt sensitivity of a grazing incidence confocal unstable resonator with applications to free electron lasers" , IEEE J. Quantum Electronics, QE-23, 229-233, (1987).
4. A. H. Paxton and W. P. Latham, Jr., "Unstable resonators with 90° beam rotation", Applied Optics, 25(17), 2939-2946, (1986).
5. R. W. Jones, C. Cason and J. F. Perkins, "New laser resonator with unobscured reflective outcoupling and internal optic axis", Paper presented at the AIAA 19th Fluid Dynamics, Plasma Dynamics, and Laser Conference, held in Honolulu, Hawaii, June 8-10, (1987).
6. B. D. McVey, "Three-dimensional simulations of free electron laser physics", Nucl. Instrum. Methods in Phy. Res., A250, 449-455, (1986).
7. E. A. Sziklas and A. E. Siegman, "Mode calculations in unstable resonators with flowing saturable gain. II: Fast fourier transform method", Applied Optics, 14(8), 1874-1889, (1975).
8. D. B. Rensch and A. N. Chester, "Iterative diffraction Calculations of transverse mode distributions in confocal unstable laser resonators", Applied Optics, 12(5), 997-1010, (1973).
9. A. H. Paxton, "Unstable resonators with negative equivalent fresnel numbers", Optics Letters, 11, 76-78, (1985).
10. M. E. Rodgers and J. H. Erkkila, "Resonator mode analysis using linear prolate functions", Applied Optics, 22(13), 1992-1995, (1983).
11. B. D. McVey with R. W. Warren, "Bending and focusing effects in a FEL oscillator II: Numerical simulations", Nucl. Instrum. Methods in Phy. Res., A259, 158-162, (1987).

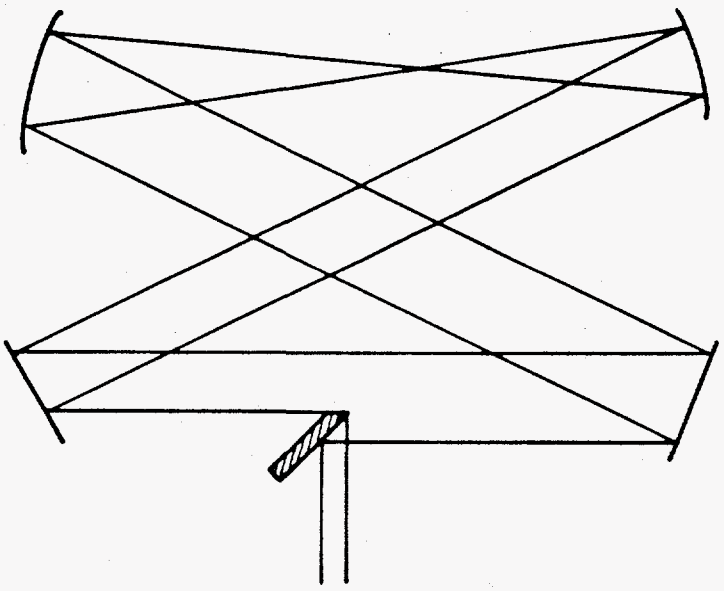

Figure 1. Stable-unstable ring with asymmetric edge scraper.

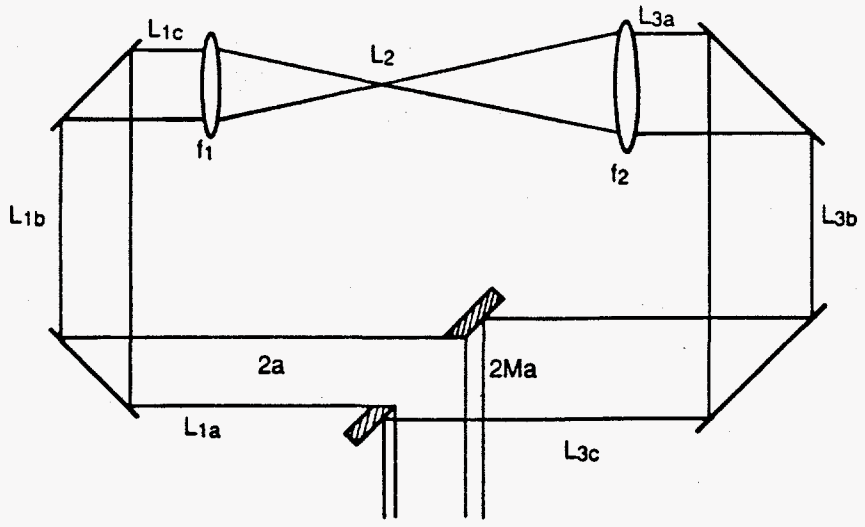

Figure 2. Unstable ring resonator with symmetric halo scraper.

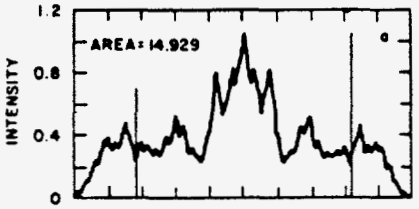

(a)

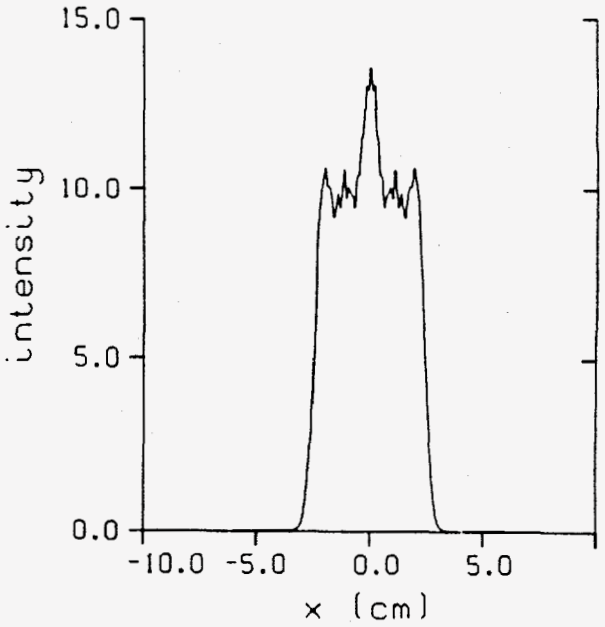

(b)

Figure 3. (a) Mode profile for $M = 1.42$, $N_{eq} = 3.12$ unstable resonator from Rensch and Chester[6]; and (b) Simulation of a negative branch unstable ring resonator with the same magnitude parameters.

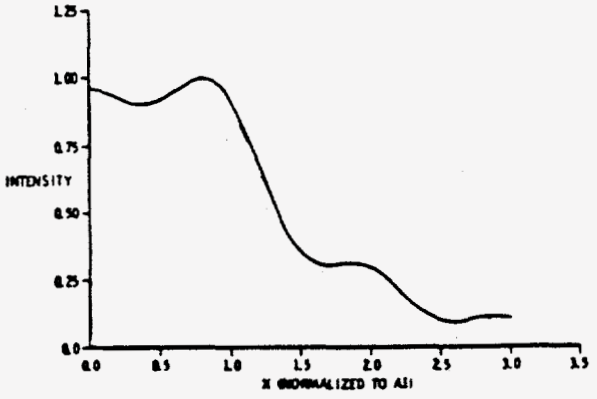

(a)

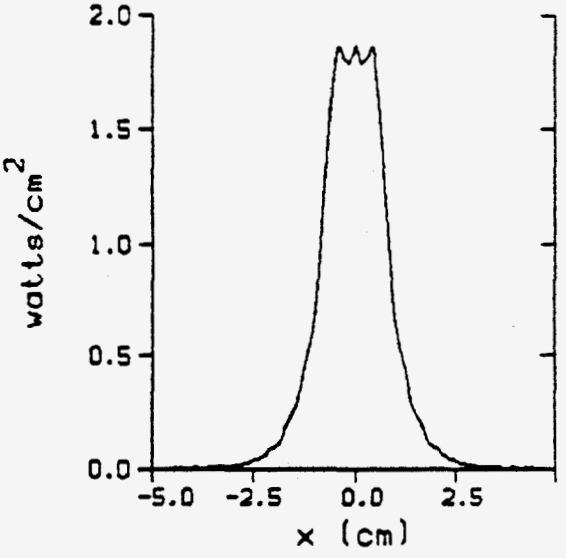

(b)

Figure 4. (a) Analytically obtained mode profile of a $M = 2.5$, $N_{eq} = 3.12$ unstable resonator from Rodgers and Erkkila[7]; and (b) Simulation of a negative branch unstable ring resonator with the same magnitude parameters.

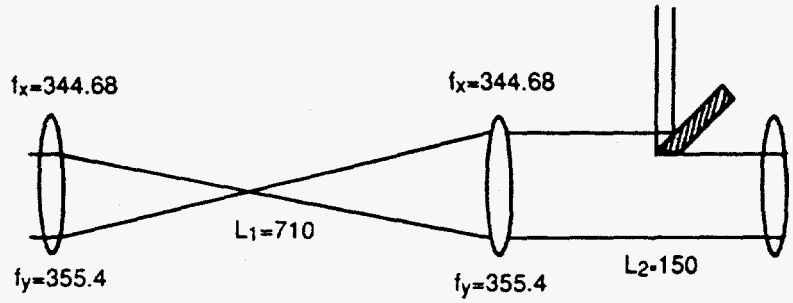

Figure 5. Equivalent stable-unstable model of the experimental resonator with asymmetric scraper.

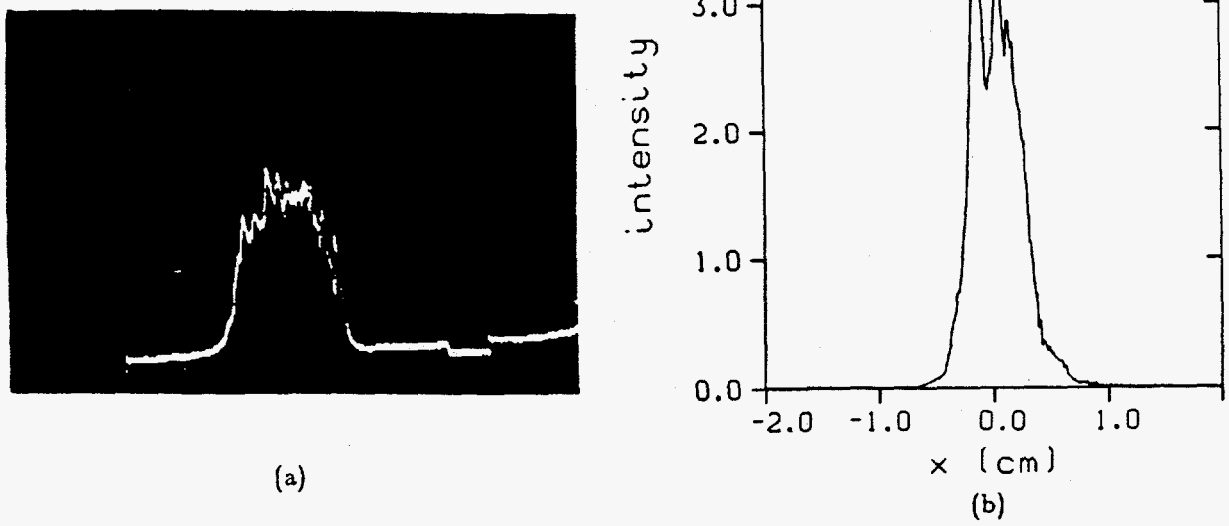

Figure 6. (a) Experimental mode profile in the unstable direction taken at one of the mirrors; and (b) mode profile at the same position from the simulation.

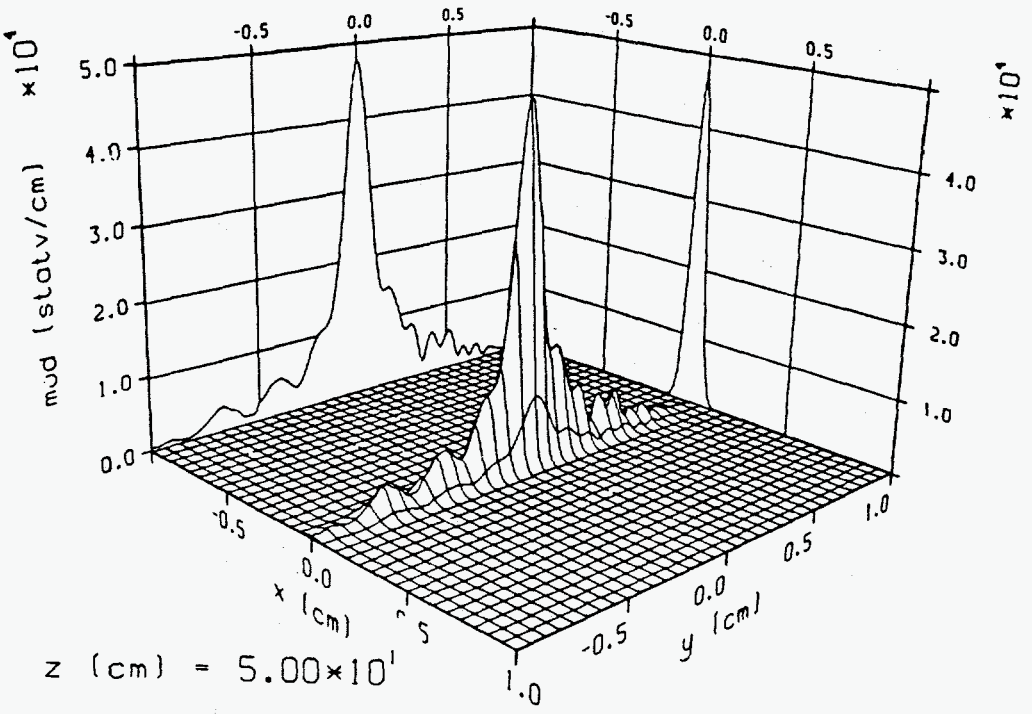

Figure 7. Three-dimensional transverse electric field profile of the stable-unstable FEL oscillator near the intracavity focus.

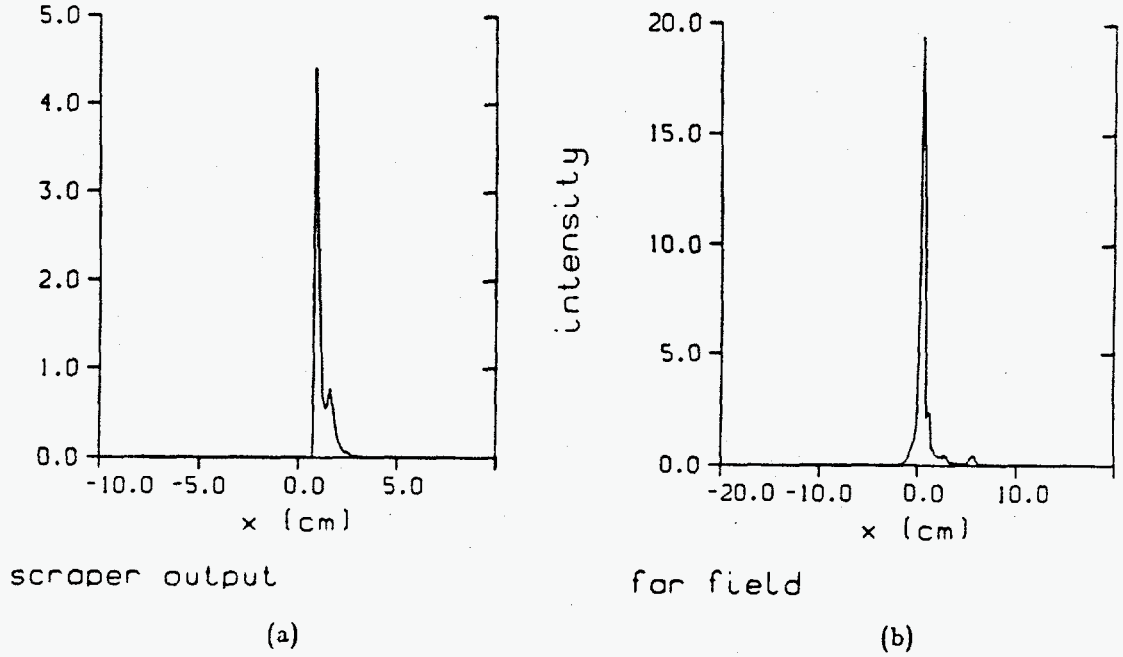

Figure 8. (a) Output beam of the stable-unstable FEL oscillator; and (b) far field pattern of the output beam in (a).

Quantum Electronics Letters

Sideband Instability in Free-Electron Lasers—A New Technique for Suppression

ALAN H. PAXTON AND MARK J. SCHMITT

Abstract—**We describe an optical element that causes very large aperture losses at the sideband frequency in a free-electron laser. The center frequency is not affected. The scheme requires the frequency width at the center frequency to be much less than the offset of the sideband radiation.**

THE sideband instability can broaden the frequency width of free-electron lasers and decrease their efficiency due to the detrapping of electrons [1]–[3]. Several techniques have already been proposed for the suppression of the sideband radiation. The sidebands were suppressed in an FEL by replacing an end mirror in a standing-wave stable cavity by a Littrow grating [4]. A diffraction-grating rhomb is a device that can be used to suppress sideband oscillations in a ring resonator [5], [6]. The grating rhomb is also used as an outcoupling element. If the grating rhomb is not needed for sideband suppression, a different outcoupling method may be preferable for some applications. For example, the stable–unstable resonator with a scaper mirror only on one side of the beam may be used [7], [8]. The fully unstable resonator has also been proposed [9]–[12], as has the unstable resonator with 90° field rotation [13]. Here, we shall discuss the stable resonator and the stable–unstable resonator as examples for the application of our new device.

Our method for sideband suppression is based on the existence of a low-pass spatial-frequency filter in the resonator. Concepts for high-energy free-electron lasers already include a spatial filter as part of the resonator. The optical beam must have a small diameter in the wiggler region; its diameter is typically larger by at least a factor of ten in some other section of the resonator. Focusing the beam and propagating it through the beam tube inside the wiggler acts as a spatial filter [14]–[15]. Increasing the spatial frequency content of the sideband light above the cutoff frequency of the spatial filter while maintaining nearly diffraction-limited performance at the central frequency would discriminate against the sideband radiation due to its higher losses at the spatial filter. Oscillation at the sideband frequency would be driven below threshold by an increase in the round-trip loss that would cause it to exceed the round-trip gain.

An optical element that would do this is a flat or spherical mirror with sections raised relative to the reference surface. The height of the raised areas would be an integral number of half wavelengths at the center frequency divided by the cosine of the angle of incidence. The height would be selected to cause substantial variations in the phase fronts of reflected sideband light. In contrast to conventional gratings, the widths of the steps are on the order of the optical beam width.

For concreteness, consider the stable resonator shown in Fig. 1. The resonator is an almost concentric, standing-wave, stable resonator. Suppose that the center wavelength is λ_c and that the sideband is at $\lambda_s = \lambda_c + \Delta\lambda$. Now suppose that mirror 1 of Fig. 1 is replaced by the phase grating shown in Fig. 2. It has the same curvature, but (for normal incidence) it has periodic steps of height

$$\Delta z = \tfrac{1}{2} n\lambda_c \tag{1}$$

where n is an integer for which

$$n = \frac{\alpha\lambda_s}{\Delta\lambda} \tag{2}$$

and α is a constant to be chosen.

Typical values are $\lambda_c = 1.0\ \mu$m and $\Delta\lambda = 0.01\ \lambda_c$. Using these values and choosing $\alpha = 0.5$ gives $n = 50$ and $\Delta z = 25\ \mu$m. Reflection of a spherical wave of wavelength λ_c from the phase grating causes no aberration because the difference in path length of any of the steps is an integral number of half wavelengths. We have assumed that the step height is much less than the pulse length of the FEL so that effects due to the finite pulse length may be ignored. Reflection of a spherical wave of wavelength λ_s from the mirror aberrates it severely, introducing a phase shift of $2\pi\alpha$ for every half period of the

Manuscript received June 22, 1989; revised March 7, 1990. This work was supported by the Strategic Defense Initiative Organization under the Small Business Innovative Research Program.

A. H. Paxton is with the Mission Research Corporation, Albuquerque, NM 87106.

M. J. Schmitt is with the Los Alamos National Laboratory, Los Alamos, NM 87545.

IEEE Log Number 9035986.

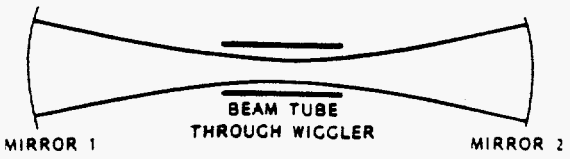

Fig. 1. Stable resonator showing beam tube through wiggler in the vicinity of the waist.

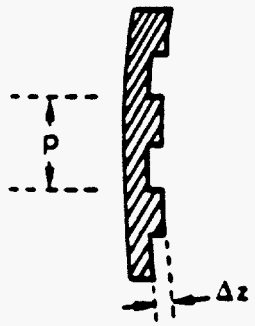

Fig. 2. Phase-step mirror. The steps are raised a distance Δz above the spherical reference surface. The step height is selected to shift the phase fronts of light at the center frequency by an integral number of wavelengths, and to cause significant phase shifts at the sideband frequency.

mirror step pattern. We shall refer to this phase grating with multiwavelength steps and a very low period as the phase-step mirror.

We will now derive some properties of the mode at the sideband frequency for the resonator in Fig. 1 with a phase-step end mirror. We assume that the light beam of the mode that is incident on the phase-step mirror is an unaberrated spherical wave. We will show that the following points are true.

1) The beam of light immediately after reflection from the phase-step mirror can be decomposed into a series of spherical waves; a zero-order wave propagates along the resonator optic axis, and the other waves propagate along axes that are tilted with respect to the optic axis.

2) A period can be derived for the phase steps such that the foci of all the tilted waves fall well outside the FEL beam tube that extends through the wiggler. Thus, only the unaberrated zero-order wave arrives to reflect from the phase-step mirror after a round-trip through the resonator, justifying our initial assumption.

3) The fractional loss of the sideband radiation at the wiggler approaches 1.0 as α approaches 0.5.

Consider a beam of light reflecting at normal incidence from the phase-step mirror shown in Fig. 2. The complex amplitude before reflection is

$$U' = F' \exp\left[i(kz - \omega t)\right] \tag{3}$$

and the complex amplitude after reflection is

$$U = F \exp\left[i(kz - \omega t)\right]. \tag{4}$$

Before reflection, the phase fronts are unaberrated and have radius of curvature r,

$$F' = u(x, y) \exp\left[\frac{-ik(x^2 + y^2)}{2r}\right]. \tag{5}$$

The complex amplitude after reflection from the phase-step mirror is

$$F = \begin{cases} u(x, y) \exp\left[\dfrac{-ik(x^2 + y^2)}{2R}\right] \exp(-i\alpha\pi) \\ \quad \text{for } (n-1)p/2 < x \le np/2 \\ u(x, y) \exp\left[\dfrac{-ik(x^2 + y^2)}{2R}\right] \exp(i\alpha\pi) \\ \quad \text{for } np/2 < x \le (n+1)p/2 \end{cases} \tag{6}$$

where n is any even integer, and a constant phase shift has been dropped. It is assumed that the steps continue over the entire region where the beam has appreciable intensity so that (6) corresponds to $u(x, y) \exp[-ik(x^2 + y^2)/2R]$ multiplied by an infinite periodic function of x. Equation (6) can be expanded as a Fourier series,

$$F = u(x, y) \exp\left[\frac{-ik(x^2 + y^2)}{2R}\right] \cdot \left[\cos\phi + i \sin\phi \sum_{m=1}^{\infty} a_m \sin(mk_t x)\right] \tag{7}$$

where $a_m = 4/m\pi$ for m odd, and $a_m = 0$ for m even. The fundamental spatial frequency is $k_t = 2\pi/p$; the longitudinal wavenumber is $k = 2\pi/\lambda_s$; half the magnitude of the phase steps imposed on the reflected beam is $\phi = \pi\alpha$; $u(x, y)$ is the amplitude of the beam, not including the spherical curvature, before reflection; R is the radius of curvature of the phase fronts after reflection. The component at spatial frequency mk_t is

$$f_m = \frac{1}{2} u(x, y) \exp\left[\frac{-ik(x^2 + y^2)}{2R}\right] a_m \sin\phi \cdot \left[\exp(imk_t x) - \exp(-imk_t x)\right]. \tag{8}$$

The wave corresponding to the first term in brackets is

$$f_m^+ = \frac{1}{2} u(x, y) \exp\left(\frac{-iky^2}{2R}\right) a_m \sin\phi \cdot \exp\left[\frac{-ik(x - x_0)^2}{2R}\right] \exp\left(\frac{im^2 k_t^2 R}{2k}\right), \tag{9}$$

where $x_0 = mk_t R/k$. Equation (9) is a tilted spherical wave with its focus offset by x_0 from the focus of the zero-frequency component. The second term in square brackets of (8) is also a tilted spherical wave, but its focus is offset by $-x_0$. Thus, the spatial frequency components imposed on the sideband radiation are shifted laterally out of the main optical beam in the vicinity of the focus, which is located a distance R from the phase-step mirror.

To determine the appropriate step period, assume that $u(x, y)$ is separable and that the reflected beam is Gaussian in the x-direction,

$$u(x, y) = v(x) g(y) \tag{10}$$

and

$$v(x) = \exp\left(\frac{-x^2}{w^2}\right). \tag{11}$$

For an almost concentric resonator, R is much greater than the Rayleigh range at the waist, so the beam waist location is essentially at distance R from the phase-step mirror. The size of the waist is

$$w_0 = \frac{R\lambda}{\pi w}. \tag{12}$$

The radius of the beam tube is given by $a = \beta w_o$ where a typical value is $\beta = 2.5$. The condition for the mth component to be centered a distance w_o outside the beam tube at the waist is

$$x_o > (1 + \beta)\, w_o. \tag{13}$$

Equivalently,

$$p < \frac{m\pi w}{1 + \beta}. \tag{14}$$

For $m = 1$, this condition leads to the loss of almost all of the power in the spatial frequencies with nonzero order.

Therefore, if inequality (14) is satisfied, the feedback power of the nonzero orders may be neglected and our assumption that an unaberrated beam is incident on the phase-step mirror is justified. The resonator has the same dominant mode that it would have if the phase-step mirror were simply a spherical mirror. Reflection from the phase-step mirror converts part of the incident field to nonzero Fourier components, which are almost entirely filtered out. The only component that survives a round-trip is the zero-order Fourier term. The fractional round-trip loss of the sideband radiation can be made arbitrarily close to one, but the dominant mode is unchanged if inequality (14) is satisfied. The fraction of the sideband power fed back, given by (7), is

$$P_f = \eta \cos^2 \phi \tag{15}$$

after one round-trip through the resonator, where η is the fractional feedback power the mode would have if the phase-step mirror were replaced by a simple spherical mirror. As ϕ approaches $\pi/2$, the fractional feedback power approaches zero.

The sideband gain has a finite frequency width. The step height Δz in (1) would be selected to correspond to a value of α near 0.5 at a wavelength near the middle of the sideband gain $\lambda = \lambda_s$. The derivative of the feedback power with respect to the sideband wavelength can be obtained from (1), (2), and (15) as

$$\frac{dP_f}{d\lambda} \cong -\eta\phi \sin 2\phi/\Delta\lambda \tag{16}$$

where $\Delta\lambda$ is the wavelength separation from the center frequency to the middle of the sideband gain. For $\alpha = 0.5$ at $\lambda \cong \lambda_s$,

$$\frac{dP_f}{d\lambda} \cong \pi^2\eta(\alpha - 0.5)/\Delta\lambda. \tag{17}$$

Therefore, if any frequency λ under the sideband gain curve satisfies $|\lambda - \lambda_s| << \Delta\lambda$, then $|P_f(\lambda) - P_f(\lambda_s)|/\eta << 1$, and the resonator losses within the sideband frequency range are about the same fraction of the losses at the center frequency.

The mirror steps need not follow straight lines. This configuration was selected because simple analysis is possible. If the laser has a long enough wavelength that diamond-turned mirrors may be used, a circular step pattern may be used to increase the loss at the sideband frequency.

A phase-step mirror will suppress the sidebands in any FEL resonator if it can be included in a region where the optical beam size is much larger than its size in the wiggler. The stable–unstable ring resonator with a compact output beam [7], [8] is of interest because it overcomes undesirable properties of other resonators proposed for use with the FEL. Standing-wave resonators for high-energy FEL's are more sensitive to mirror tilt than ring resonators [16] because the optical beam is radially inverted twice during each round-trip propagation in a standing-wave resonator versus once in a ring. Fully unstable resonators would have undesirably large diffractive losses because the magnet faces of the wiggler are too close together to accommodate the diffractive side lobes at the focus. Stable ring resonators use a partially transparent mirror or a diffraction grating for outcoupling, which may be undesirable in a high-energy laser. The stable–unstable resonator allows reflective outcoupling of a filled-in rectangular beam. Sketches of the stable–unstable ring are shown in Figs. 3 and 4. Modes of this resonator are described in [7].

Numerical calculations were performed with the FEL simulation code FELEX [20] to obtain the power loss ratio for a stable–unstable ring cavity including a phase-step mirror. Only empty-cavity calculations were done. The dimensions of the ring are shown in Figs. 3 and 4. The steps caused phase variation only along the stable (x) direction. The optical propagation algorithm made use of a fast Fourier transform. Filtering of the high spatial frequencies was required to prevent significant aliasing. The transmission function in transform space was

$$T_k = 1 \quad \text{for} \quad |k_t| < k_{ap}$$

and

$$T_k = \frac{1}{2}\left[1 + \cos\left(\frac{\pi(|k_t|/k_{\max} - k_{ap}/k_{\max})}{1 - k_{ap}/k_{\max}}\right)\right]$$

$$\text{for} \quad |k_t| > k_{ap} \tag{18}$$

where $k_{\max}$ is the maximum spatial frequency of the grid for the discrete Fourier transform, and, for these simulations, $k_{ap}/k_{\max} = 0.85$.

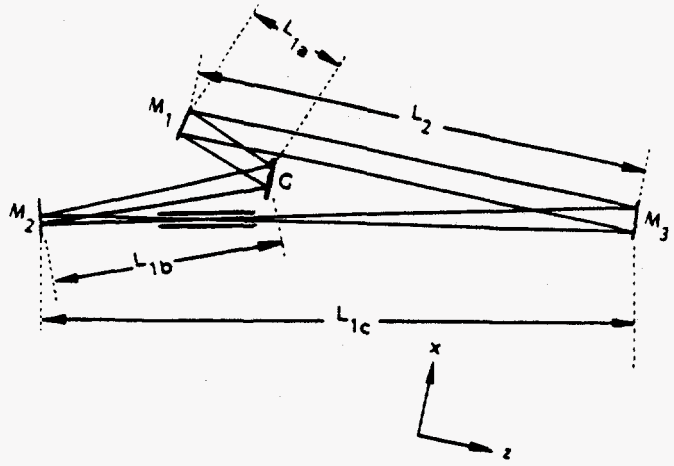

Fig. 3. Stable-unstable ring resonator with a phase-step mirror. The traveling-wave optical beam is rectangular in cross section. The stable direction is shown. For clarity, the optical elements are shown as offset, but the optic axis is really contained in a single plane of constant x. Mirrors M_1 and M_3 are curved in this dimension and M_2 is a flat mirror. The phase-step mirror is labeled G. Dimensions are $L_1 = L_{1a} + L_{1b} + L_{1c} = 7100$ cm and $L_2 = 1500$ cm. In doing the calculation, it was assumed that L_{1a} was negligible in comparison to L_1. The focal lengths of the curved mirrors are $F_1 = F_3 = 3554$ cm in this dimension. The Gaussian beam size is $w = 1.33$ cm in the region with length L_2. The wavelength used in the simulation was 0.593 μm.

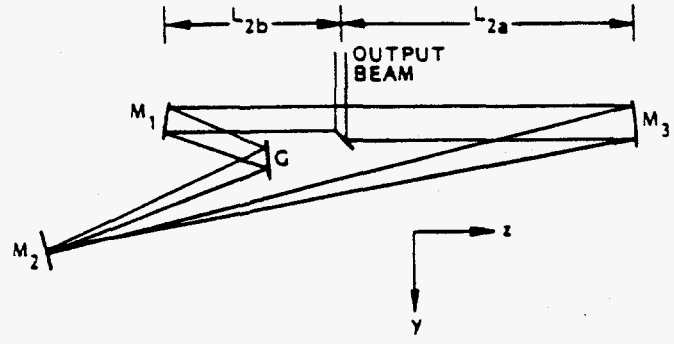

Fig. 4. Stable-unstable ring resonator with a phase-step mirror. Unstable direction is shown. Dimensions not shown in Fig. 3 are $L_{2a} = 750$ cm, $L_{2b} = 750$ cm, and the beam width just after the scraper is $h = 1.49$ cm. The mirror focal lengths in this dimension are $F_1 = F_3 = 3446.8$ cm. Different focal lengths in the two dimensions could be obtained by selecting the angle of incidence for the beam at spherical mirrors to induce the required astigmatism [17]. The resonator magnification is $M = -1.36$, and the equivalent fresnel number [10], [18], [19] is $N_{eq} = -0.38$.

The simulations consisted of propagating an initial complex electric-field amplitude around the resonator (including the phase-step mirror) until a constant loss per pass was achieved. 20 passes were usually sufficient. The half-width of the beam tube through the wiggler was $a = 2.5w_o$ in the stable direction. The period of the phase-step mirror was $p = 0.30w$. A plot of the fractional round-trip power loss as a function of the angular shift of the phase fronts due to reflection from the phase-step mirror is shown in Fig. 5. Although the maximum loss will occur in the vicinity of π radians, simulations with phase shift greater than $\pi/2$ rad could be performed due to numerical difficulties. Results plotted in Fig. 5 may be compared

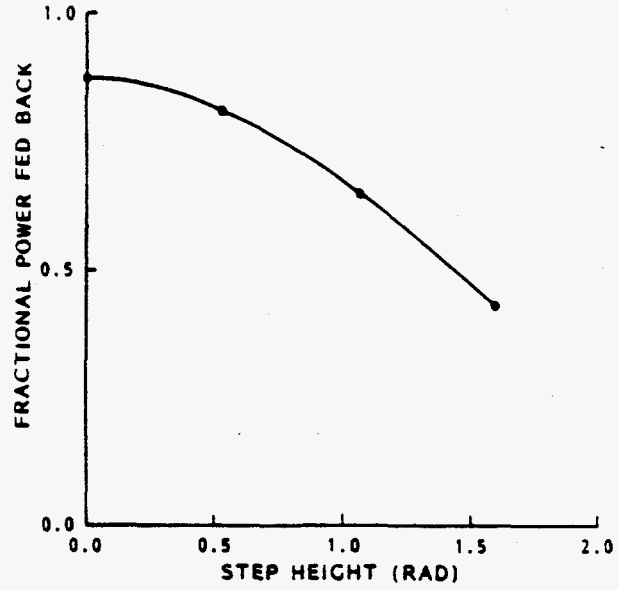

Fig. 5. Fractional power fed back as a function of the step height induced on the phase fronts of the optical beam by reflection from the phase-step mirror.

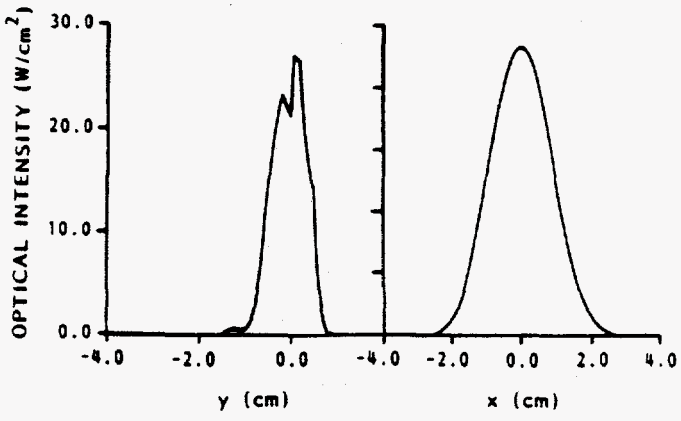

Fig. 6. Optical intensity just past the plane of reflection from the phase-step mirror.

with the simple theory derived above. The point at $\phi = 0$ in Fig. 5 gives $\eta = 0.875$. Values of P_f obtained from (15) agree with the second and third points from the left on Fig. 5 to within 0.4 percent. The right-hand point on Fig. 5 agrees with (15) to within 1%. Plots of the electric-field intensity and phase immediately after reflection from the phase-step mirror are given in Figs. 6 and 7. Note the phase steps introduced by the phase-step mirror. These phase variations caused the field intensity oscillations shown in Fig. 8 after propagating approximately two-thirds of the distance to the focus. The field just in front of the wiggler is given in Fig. 9. The two side lobes were caused by the two titled plane waves corresponding to the fundamental spatial frequency of the phase-step mirror. Since an aperture was imposed at ± 0.2 cm, the side lobes were prevented from propagating through the wiggler. As the phase step height moved toward π radians, the side lobe amplitude increased at the expense of the central

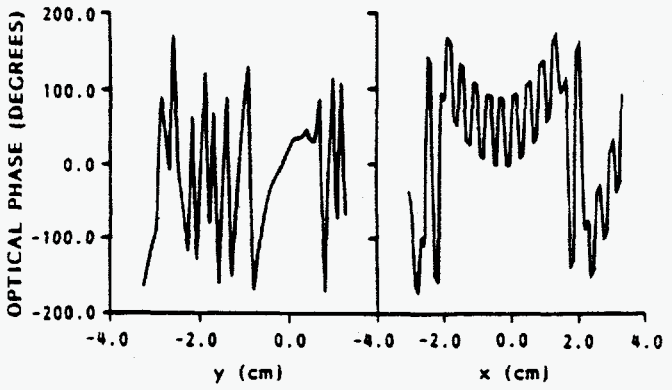

Fig. 7. Phase of optical beam just past the plane of reflection from the phase-step mirror.

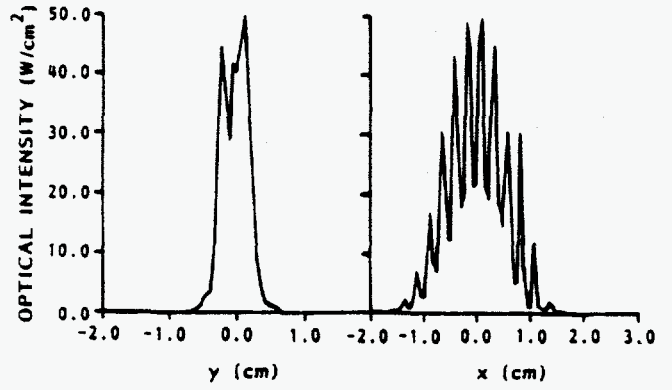

Fig. 8. Optical intensity at location two-thirds of the way from mirror M_1 to the focus.

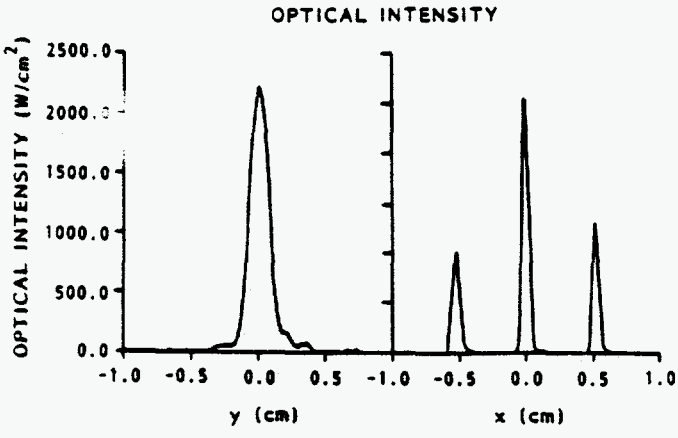

Fig. 9. Optical intensity at the entrance to the wiggler. The edges of an aperture were located at $x = \pm 0.2$ cm.

lobe. Losses would be extremely high for phase shifts near π radians.

A phase-step mirror could be used in a slightly different way to discriminate against the sideband radiation. A phase-step mirror with a period equal to its width might not cause sufficient losses at apertures for suppression, but destructive interference would decrease the intensity at the electron beam location, thereby decreasing the coupling between the optical beam and the electron beam. The use of a "grating" with a single step for sideband suppression has already been suggested [21].

A resonator could be designed with a configuration similar to the Boeing burst mode resonator [22], [23] but modified to be unstable in one transverse direction. The grating rhomb could be eliminated and a phase-step mirror added, together with a flat mirror to keep the number of resonator mirrors even. Outcoupling could be achieved by adjusting the curvature of the resonator mirrors to make the resonator unstable in the transverse dimension with its axis parallel to the faces of the wiggler magnets and inserting an output coupling scraper mirror on one side of the beam.

The compact-beam, stable-unstable ring resonator with a phase-step mirror may provide a useful alternative to the stable ring resonator with a grating rhomb for high-energy FEL's.

Acknowledgment

We wish to thank J. C. Goldstein of the Los Alamos National Laboratory for bringing recent work on sideband suppression at LANL to our attention. We are indebted to C. Knapp of the Los Alamos National Laboratory for suggesting that a diamond-turned element might substitute for the straight-grooved phase-step mirror.

References

[1] N. M. Kroll and M. N. Rosenbluth, "Sideband instabilities in trapped particle free-electron lasers," in *Free-Electron Generators of Coherent Radiation*, S. F. Jacobs, H. S. Pilloff, M. Sargent III, M. O. Scully, and R. Spitzer, Ed. Reading, MA: Addison-Wesley, 1980, pp. 147-174.

[2] J. C. Goldstein, "Evolution of long pulses in a tapered-wiggler free-electron laser," *Proc. SPIE, Free-Electron Generators of Coherent Radiation*, C. A. Brau, S. F. Jacobs, and M. O. Scully, Eds., vol. 453, pp. 2-10, 1984.

[3] D. C. Quimby, J. M. Slater, and J. P. Wilcoxon, "Sideband suppression in free-electron lasers with multiple synchrotron periods," *IEEE J. Quantum Electron.*, vol. QE-21, pp. 979-987, 1985.

[4] J. E. Sollid, D. W. Feldman, R. W. Warren, H. Takeda, S. J. Gitomer, W. J. Johnson, and W. E. Stein, "Sideband suppression in the Las Alamos free-electron laser using a Littrow grating," presented at the *1988 Free-Electron Laser Conf.*, Jerusalem, Israel, Aug. 29-Sept. 2, 1988.

[5] R. L. Tokar, B. D. McVey, and J. C. Goldstein, "Sideband suppression in free-electron lasers using a grating rhomb," *IEEE J. Quantum Electron.*, vol. 24, pp. 856-863, 1988.

[6] V. K. Viswanathan, P. J. Wantuck, Q. D. Appert, D. J. Pistoresi, K.-O. Tong, "Rhomb gratings for sideband suppression," presented at Opticon '88, Santa Clara, CA, Oct. 30-Nov. 4, 1988.

[7] M. J. Schmitt and A. H. Paxton, "Free-electron lasers using stable-unstable ring resonators," *SPIE, Symp. Lasers and Opt.*, Jan. 15-20, 1989, vol. 1045, pp. 36-43.

[8] R. W. Jones, C. Cason, and J. F. Perkins, "New laser resonator with unobscured reflective outcoupling and internal optic axis," presented at *AIAA 19th Fluid Dynamics, Plasma Dynamics, Lasers Conf.*, Honolulu, HI, June 8-10, 1987.

[9] G. T. Moore, "Unstable resonators for the free-electron laser," *Proc. SPIE, Free Electron Generators of Coherent Radiation*, C. A. Brau, S. F. Jacobs, M. O. Sculley, Eds., vol. 453, pp. 255-260, 1984.

[10] A. H. Paxton, "Unstable resonators with negative equivalent Fresnel numbers," *Opt. Lett.*, vol. 11, pp. 76-78, 1986.

[11] E. Sklar, "The advantages of a negative branch unstable resonator for use with free-electron lasers," *IEEE J. Quantum Electron.*, vol. QE-22, pp. 1088–1094, 1986.

[12] P. K. Kennedy, K. C. Sun, R. H. Labbe, and R. A. Cover, "Effect of various outcoupling options on free-electron ring laser performance," *IEEE J. Quantum Electron.*, vol. 25, pp. 2322–2326, 1989.

[13] R. W. Jones and J. F. Perkins, "Transverse mode properties of beam-rotated unstable resonators for free electron lasers," *J. AIAA*, vol. 26, pp. 897–900, 1988.

[14] K. E. Oughstun, "Unstable resonator modes," in *Progress in Optics*, vol. XXIV, E. Wolf, Ed. Amsterdam, The Netherlands: North-Holland, 1987, sect. 3.4.2.

[15] P. G. Gobbi and G. C. Reali, "A novel unstable resonator configuration with a self filtering aperture," *Opt. Commun.*, vol. 52, pp. 195–198, 1984.

[16] J. M. Eggleston, "Angularly stable ring resonators for high power FEL's," in *Proc. Int. Conf. Lasers* '83, Dec. 12–16, R. C. Powell, Ed. McLean, VA: STS, 1983.

[17] C. Cason, R. W. Jones, and J. F. Perkins, "Unstable optical resonators with tilted spherical mirrors," *Opt. Lett.*, vol. 2, pp. 145–147, 1978.

[18] A. E. Siegman, *Lasers*. Mill Valley, CA: Univ. Science, 1986, pp. 872–873.

[19] A. H. Paxton and W. P. Latham, Jr., "Unstable resonators with 90° beam rotation," *Appl. Opt.*, vol. 25, pp. 2939–2946, 1986, eq. (35).

[20] B. D. McVey, "Three-dimensional simulations of free electron laser physics," *Nucl. Instr. and Meth.*, vol. A250, pp. 449–455, 1986.

[21] J. E. Sollid, D. W. Feldman, and R. W. Warren, "Sideband suppression for free-electron lasers," presented at *Proc. 1988 Free-Electron Laser Conf.*, Jerusalem, Israel, Aug. 29–Sept. 2, 1988.

[22] S. V. Gunn and K. C. Sun, "Design of ring resonator for burst mode free electron laser," *AIAA '87 Conf.*, Honolulu, HI, June 8–10, 1987, AIAA-87-1280.

[23] C. E. Knapp, V. K. Viswanathan, and Q. D. Appert, "Analysis of the Boeing FEL mirror measurements," *Proc. SPIE, Symp. Lasers and Optics*, Jan. 15–20, 1989, vol. 1047.